國立交通大學

電機與控制工程研究所

碩士論文

快速輻射半徑基底函數網路演算法
於蛋白質相對溶劑可接觸性預測的應用

Applying Quick Radial Basis Function Network
to Protein Relative Solvent Accessibility Prediction

學生：游涵任

指導教授：張志永

中華民國九十五年七月

快速輻射半徑基底函數網路演算法

於蛋白質相對溶劑可接觸性預測的應用

Applying Quick Radial Basis Function Network
to Protein Relative Solvent Accessibility Prediction

學　　生：游涵任	Student : Han-Jen Yu
指導教授：張志永	Advisor : Jyh-Yeong Chang

國立交通大學

電機與控制工程學系

碩士論文

A Thesis

Submitted to Department of Electrical and Control Engineering

College of Electrical Engineering and Computer Science

National Chiao Tung University

in Partial Fulfillment of the Requirements

for the Degree of Master in

Electrical and Control Engineering

July 2006

Hsinchu, Taiwan, Republic of China

中華民國九十五年七月

快速輻射半徑基底函數網路演算法
於蛋白質相對溶劑可接觸性預測的應用

學生:游涵任　　　　　　　　　　　　指導教授:張志永博士

國立交通大學電機與控制工程研究所

摘要

蛋白質在生物體中一直扮演著很重要的角色,蛋白質被發現的數量及其結構逐年增加。隨著蛋白質的應用越來越廣泛，待解決的課題也就越來越多。例如：蛋白質二級結構預測問題、蛋白質相對溶劑可接觸性預測問題等。目前在蛋白質結構問題的解決上,科學家都是利用X光繞射以及核磁共振（NMR）來取得實驗結果。這些方法雖然正確率高，但是相對地所要花費的時間及成本是相當高的。因此利用電腦科學中的機器學習（Machine learning）演算法來預測這些問題，相信能夠有效降低實驗與時間成本。

本篇論文，我們利用修改的快速輻射半徑基底函數網路演算法，混合從PSI-BLAST 產生的位置加權矩陣，針對蛋白質相對溶劑可接觸性預測問題進行研究。最近歐等人［10］，發展出快速輻射半徑基底函數網路演算法，是一種較快速且精確設計之網路，應用於蛋白質二級結構預測有顯著的效果。我們的修改的

快速輻射半徑基底函數網路演算法，應用於蛋白質相對溶劑可接觸性預測。我們使用五種不同的快速輻射半徑基底函數網路演算法，應用在三態相對溶劑可接觸性預測和二態相對溶劑可接觸性預測。此五種方法包括:(1) 快速輻射半徑基底函數網路演算法、(2) 二階快速輻射半徑基底函數網路演算法、(3) 一般混合快速輻射半徑基底函數網路演算法、(4) 地域趨勢混合快速輻射半徑基底函數網路演算法、以及(5) 全域趨勢混合快速輻射半徑基底函數網路演算法。我們選擇有最佳表現的一般混合快速輻射半徑基底函數網路演算法，做為建議的演算法。我們也將修改的快速輻射半徑基底函數網路演算法的實驗結果，與近幾年的其他方法比較，並且提出我們的方法改進方向的建議。

Applying Quick Radial Basis Function Network to Protein Relative Solvent Accessibility Prediction

STUDENT: HAN-JEN YU ADVISOR: JYH-YEONG CHANG

Institute of Electrical and Control Engineering

National Chiao-Tung University

Abstract

Proteins have been played an important role in a creature and the numbers of proteins and their structures have been increased with years. Since protein applications are more widely used, there will be a lot of problems to be solved. For example, there are protein secondary structure prediction problem, protein relative solvent accessibility problem and so on. Nowadays, scientists use X-ray diffraction or nuclear magnetic resonance (NMR) to solve the protein structure problem. Although they can achieve high accuracy, it is expensive and long to solve this protein problem. To reduce the time and the costs, it is imperative to use machine learning algorithms to solve this protein problem.

In this thesis, we study protein relative solvent accessibility problem using a modified QuickRBF method combined with a position-specific scoring matrix (PSSM) generated from PSI-BLAST. The QuickRBF method, recently developed by Ou *et al.* [10], has been applied to protein secondary structure prediction with excellent results. Our modified QuickRBF method is applied on relative solvent accessibility prediction. Five different kind of QuickRBF approaches are applied on three-state, E, I, and B, and two-state, E, and B, relative solvent accessibility predictions. These five approaches include: (1) QuickRBF, (2) Two-Stage QuickRBF, (3) Common Fusion QuickRBF, (4) Local Tendency Fusion QuickRBF, and (5) Global Tendency Fusion QuickRBF. We recommend the Common Fusion QuickRBF approach which has the best performance as our modified QuickRBF method. We also compare the results of the modified QuickRBF method with other methods in the recent years, and suggest the improvement direction of our approach in the future.

Acknowledgement

I would like to express my sincere appreciation to my advisor, Dr. Jyh-Yeong Chang. Without his patient guidance and inspiration during the two years, it is impossible for me to overcome the obstacles and complete the thesis. In addition, I am thankful to all my lab members for their discussion and suggestion.

Finally, I would like to express my deepest gratitude to my family. Without their strong support and encouragement, I could not go through the two years.

Contents

List of Figures

List of Tables

Chapter 1. Introduction

1.1 Motivation and The Background of This Research

The knowledge of protein structures is valuable for understanding mechanisms of diseases of living organisms and for facilitating discovery of new drugs. Protein structure can be experimentally determined by NMR spectroscopy and X-ray crystallography techniques or by molecular dynamics simulations. However, the experimental approaches are marred by long experimental time, prone to difficulties, and expensive. There are more than 130,000 protein sequences in Swissport (release 41.20), but less than about 37,000 three-dimensional (3D) protein structure are in the Protein Data Bank (PDB). Only a small fraction, 17%, of the enormous number of sequenced proteins has their structure determined. In order to reduce the gap between sequence and structure, developing reliable and applicable structure prediction method has become a more important task in computational biology. An intermediate but useful step is to predict protein secondary structure (PSS) or relative solvent accessibility (RSA), which provides some knowledge and simplifies the complicated 3D structure prediction problem [1], [2]. The usual goal of RSA prediction is to classify a pattern of residues in amino acid sequences to a pattern of solvent accessibility elements: buried (B), intermediate (I) and exposed (E) residues. Though the prediction of solvent accessibility is less accurate than that of secondary structure from the homology approach, since it is less conserved than secondary structure [3], there has been much effort to improve prediction accuracy to obtain important information regarding a buried, intermediate or exposed residue for constructing tertiary structure from sequences. Many different techniques have been proposed for RSA prediction, which broadly fall into the following categories: (1) Bayesian, (2) neural networks, and (3) information theoretical approaches. The Bayesian methods provide a framework to take into account local interactions among amino acid residues, by extracting the information from single sequences or multiple sequence alignments to obtain posterior probabilities for RSA prediction [4]. Neural networks use residues in a local neighborhood, as inputs, to predict the RSA of a residue at a particular location by finding an arbitrary, nonlinear mapping [5]–[8]. The information theoretical approaches use mutual information between the sequences of amino acids and solvent accessibility values derived from a single amino acid residue, or pairs of residues, in a neighborhood for RSA prediction [9]. In this study, we propose a modified QuickRBF method for RSA prediction combined with a position-specific scoring matrix (PSSM) generated from PSI-BLAST. The QuickRBF method, recently developed by Ou *et al.* [10], is applied on protein secondary structure prediction. Our modified QuickRBF method is applied on relative solvent accessibility prediction. We also compare the results of the modified QuickRBF method with other methods.

1.2 Thesis Outline

The organization of this thesis is structured as follows. Chapter 1 introduces the role of machine learning, the motivation and the background of this thesis. In Chapter 2, we will first introduce the data set and the definition of protein solvent accessibility. Then we will propose five different kind of QuickRBF methods to predict protein relative solvent accessibility. In Chapter 3, the experiment of computer simulation and the results are conducted and compared with other methods. Finally, the conclusion of this thesis is presented in Chapter 4.

Chapter 2. Materials and Methods

2.1 Training and Data Set

The set of 126 nonhomologous globular protein chains used in the experiment of Rost and Sander [3] and referred to as the RS126 set was used to evaluate the accuracy of the prediction. The proteins in the RS126 data set have less than 25% pairwise sequence identity. This set was used to evaluate different methods of relative solvent accessibility prediction, for example, PHDacc [3] and other methods [21]–[23]. In this paper, we performed a sevenfold cross-validation test on this set as defined in Table 2.1. In order to avoid the selection of extremely biased partitions, the RS126 set was divided into subsets of approximately same composition of each type of RSA state. One subset was chose as the testing set while the rest was merged into the training set. This procedure was repeated seven times to cover whole RS126 data set.

Table 2.1. The database of non-homologous proteins used for seven-fold cross validation. All proteins have less than 25% pairwise similarity for lengths greater than 80 residues.

Fold_A	256b_A	2aat	8abp	6acn	1acx	8adh	3ait
	2ak3_A	2alp	9api_A	9api_B	1azu	1cyo	1bbp_A
	1bds	1bmv_1	1bmv_2	3blm	4bp2		
Fold_B	2cab	7cat_A	1cbh	1cc5	2ccy_A	1cdh	1cdt_A
	3cla	3cln	4cms	4cpa_I	6cpa	6cpp	4cpv
	1crn	1cse_I	6cts	2cyp	5cyt_R		
Fold_C	1eca	6dfr	3ebx	5er2_E	1etu	1fc2_C	1fdl_H
	1dur	1fkf	1fnd	2fxb	1fxi_A	2fox	1g6n_A
	2gbp	1a45	1gd1_O	2gls_A	2gn5		
Fold_D	1gpl	4gr1	1hip	6hir	3hmg_A	3hmg_B	2hmz_A
	5hvp_A	2i1b	3icb	7icd	1il8_A	9ins_B	1l58
	1lap	5ldh	1gdj	2lhb	1lmb_3		
Fold_E	2ltn_A	2ltn_B	5lyz	1mcp_L	2mev_4	2or1_L	1ovo_A
	1paz	9pap	2pcy	4pfk	3pgm	2phh	1pyp
	1r09_2	2pab_A	2mhu	1mrt	1ppt		
Fold_F	1rbp	1rhd	4rhv_1	4rhv_3	4rhv_4	3rnt	7rsa
	2rsp_A	4rxn	1s01	3sdh_A	4sgb_I	1sh1	2sns
	2sod_B	2stv	2tgp_I	1tgs_I	3tim_A		
Fold_G	1bks_A	1bks_B	1tnf_A	1ubq	2tmv_P	2tsc_A	2utg_A
	2wrp_R	4ts1_A	4xia_A	6tmn_E	9wga_A		

2.2 The Definition of Protein Solvent Accessibility

2.2.1 Static Residue Solvent Accessibility

The native structure of globular proteins exists only in the presence of water [11], and therefore the analysis of their interactions with water is central to the theory of protein structure [12]. The term “accessible surface area” was introduced by Lee and Richards [13] to quantitatively describe the extent to which atoms on the protein surface can form contacts with water. For a particular protein atom it is defined as the area over which the centre of a water molecule can be placed while retaining van der Waals contacts with that atom and not penetrating any other atom. The principal goal is to predict the extent to which a residue embedded in a protein structure is accessible to solvent. Solvent accessibility can be described in several ways [13]–[15]. The most detailed fast method compiles solvent accessibility by estimating the volume of a residue embedded in a structure that is exposed to solvent as shown in Fig. 2.1; note: this method was developed by Lee and Richards [13] and later implemented in DSSP [16]. Different residues have a different possible accessible area.

Studies of solvent accessibility in proteins have led to many new insights into protein structure [13]–[18]. Knowledge of solvent accessibility has proved useful for identifying protein function, sequence motifs, and domains, and for formulating hypotheses about antigenic determinants, site-directed mutagenesis, humanization of antibodies, and on the correctness of designed or experimentally determined protein structures. Furthermore, knowledge of solvent accessibility has assisted alignments in regions of remote sequence identity.

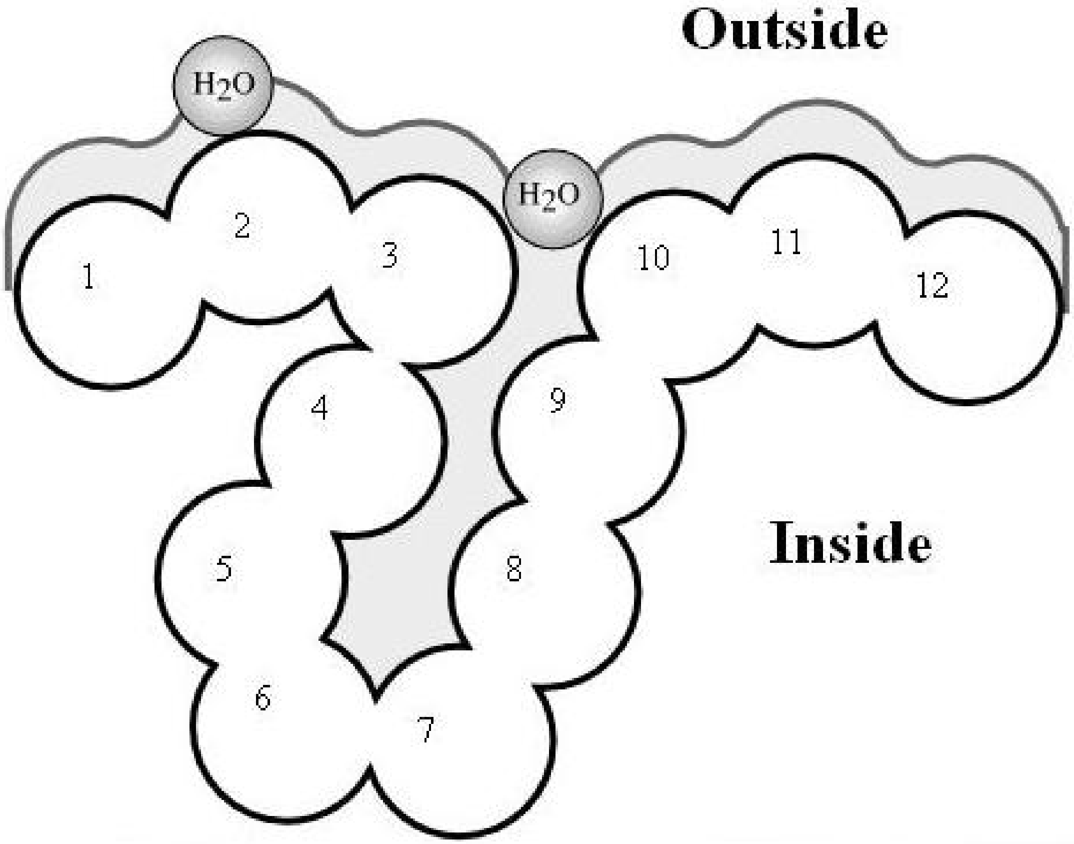

Fig. 2.1. Measure accessibility. Residue solvent accessibility is usually measured by rolling a spherical water molecule over a protein surface and summing the area that can be accessed by this molecule on each residue (typical values range from 0—300 Å^2). To allow comparisons between the accessibility of long extended and spherical amino acids, typically relative values are compiled (actual area as percentage of maximally accessible area). A more simplified description distinguishes two states: exposed (here residues numbered 1—3 and 10—12) and buried (here residues 4—9) residues. Since the packing density of native proteins resembles the crystals, values for solvent accessibility provide upper and lower limits to the number of possible inter-residue contacts.

2.2.2 Residue Relative Solvent Accessibility

How can the solvent accessibility of a residue embedded in a 3D structure be cast into a simple number? One simple way is to count the number of water molecules in direct contact with the residue, as estimated by the program DSSP for the first hydration shell. For comparison between amino acids of different sizes, the relative solvent accessibility is a useful quantity as defined in Table 2.2.

Amino acid relative solvent accessibility is the degree to which a residue in a protein is accessible to a solvent module. The relative solvent accessibility can be calculated by the formula as follows:

$$\mathrm{RelAcc}\ (\%) = 100 \times \mathrm{Acc} \,/\, \mathrm{MaxAcc}\ (\%)\ ,$$

where Acc is the solvent accessible surface area of the residue observed in the 3D structure, given in Angstrom units, calculated from coordinates by the dictionary of protein secondary structure (DSSP) program [16]. The number of water molecules around a residue can be approximated by Acc/10, and MaxAcc is the maximum value of solvent accessible surface area of each kind of residue for a Gly-X-Gly extended tripeptide conformation.

Table 2.2. Definition of solvent accessibility states.

- Solvent accessibility:

  Acc = solvent accessibility of a residue (given in Å^2) calculated from coordinates using DSSP [16]. $W \approx Acc/10$, approximates the number of water molecules around the residue.

- Relative solvent accessibility:

  RelAcc = Acc/MaxAcc, with maximal accessibility (measured in Å^2) for the amino acids given by the table following (amino acids in one-letter code; B stands for D or N; Z for E or Q, and X for an undetermined amino acid) [18][19].

AA	A	B	C	D	E	F	G	H	I	K	L	M
MaxAcc	106	160	135	163	194	197	84	184	169	205	164	188
AA	N	P	Q	R	S	T	V	W	X	Y	Z	
MaxAcc	157	136	198	248	130	142	142	227	180	222	196	

- Two-state (binary) model for accessibility (B/E) :

	Buried (B)	Exposed (E)
Thresholds to distinguish two states	RelAcc $\leq$ 0%	RelAcc > 0%
	RelAcc < 5%	RelAcc $\geq$ 5%
	RelAcc < 9%	RelAcc $\geq$ 9%
	RelAcc < 16%	RelAcc $\geq$ 16%
	RelAcc < 25%	RelAcc $\geq$ 25%

- Three-state (ternary) model for accessibility (B/I/E) :

	Buried (B)	Intermediate (I)	Exposed (E)
Thresholds to distinguish three states	RelAcc < 9%	9% $\leq$ RelAcc < 36%	RelAcc $\geq$ 36%

- Measure for evaluation of conservation and accuracy of prediction:

  Q_2 percentage of conserved, or correctly predicted, residues in two states defined by thresholds given above.

  Q_3 percentage of conserved, or correctly predicted, residues in three states defined by thresholds given above.

RelAcc can hence adopt values between 0% and 100%, with 0% corresponding to a fully buried and 100% to a fully accessible residue, respectively. Different arbitrary threshold values of relative solvent accessibility are chose to define categories: buried and exposed as shown in Fig. 2.2, or ternary categories: buried, intermediate, or exposed. The precise choice of the threshold is not well defined [3].

We used two kind of class definitions: (1) buried (B) and exposed (E); and (2) buried (B), intermediate (I), and exposed (E). For the two-state, B and E definition, we chose various thresholds of the relative solvent accessibility such as 25%, 16%, 9%, 5%, and 0%. For the three-state, B, I, and E, description of relative solvent accessibility, one set of thresholds that we selected is the same as those in Rost and Sander [3]:

Buried (B): RelAcc < 9%

Intermediate (I): 9% ≤ RelAcc < 36%

Exposed (E): RelAcc ≥ 36%

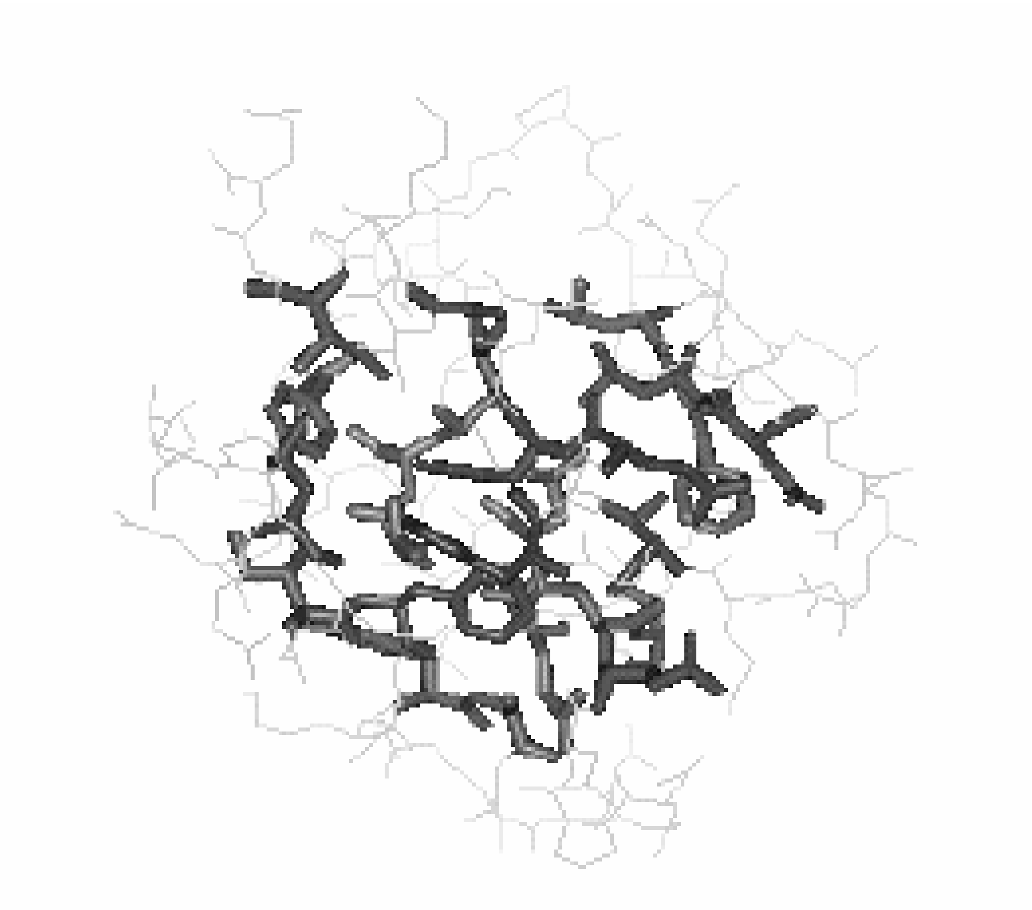

Fig 2.2. Binary model: thick and dark line is buried residues; thin and light line is exposed residues [20].

2.3 PSI-BLAST Profiles

It is well known that evolutionary information in the form of multiple alignments and profiles significantly improves the accuracy of, for instance, secondary structure prediction methods [4], [24]–[27]. This is so because the secondary structure of a family is more conserved than the primary amino acid sequence. Similar effects have been reported for the prediction of contact number and relative solvent accessibility. For relative solvent accessibility, a corresponding increase of 5% has been described both with neural networks [25] and Bayesian methods.

PSI-BLAST [28] generates the profile of a protein in the form of an $N\times20$ position-specific scoring matrix as shown in Fig. 2.3, where N is the length of the sequence. PSI-BLAST is run with default options, -j 3, -h 0.001, and -e 10.0, and the non-redundant protein sequence database (ftp://ncbi.nlm.nih.gov/blast/db) filtered by PFILT [29] to mask out regions of low complexity sequence, the coiled coil regions and transmembrane spans. The BLOSUM62 [30] substitution matrix as shown in Fig. 2.4, is used for PSI-BLAST. These profiles were scaled to the required 0–1 range using the standard logistic function:

$$f(x) = \frac{1}{1+\exp(-x)} \quad ,$$

where x is the raw profile matrix value.

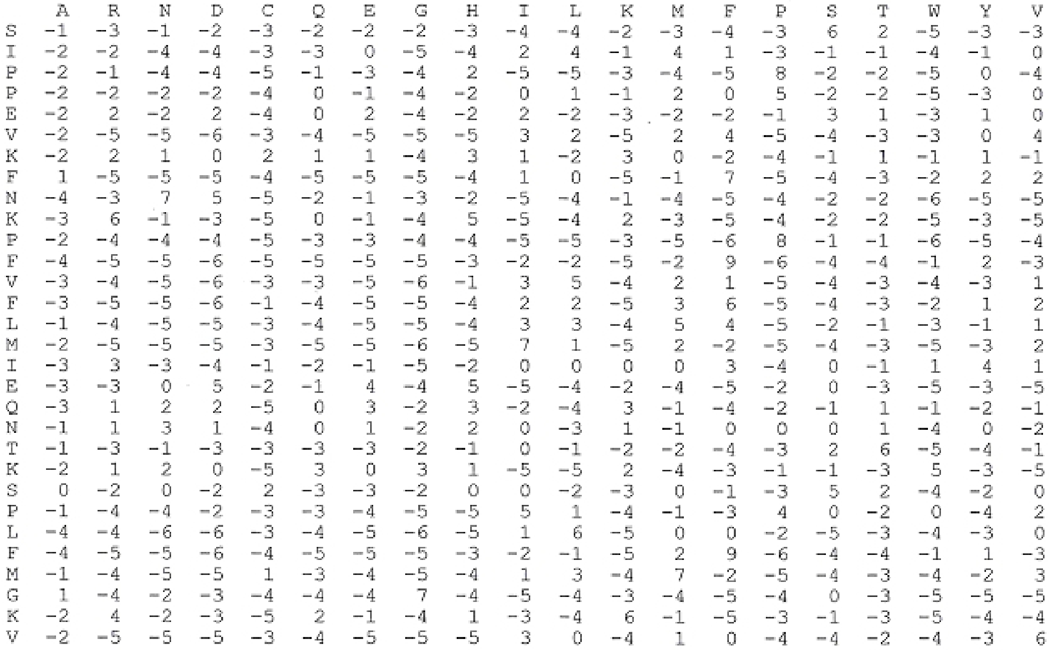

	A	R	N	D	C	Q	E	G	H	I	L	K	M	F	P	S	T	W	Y	V
S	-1	-3	-1	-2	-3	-2	-2	-2	-3	-4	-4	-2	-3	-4	-3	6	2	-5	-3	-3
I	-2	-2	-4	-4	-3	-3	0	-5	-4	2	4	-1	4	1	-3	-1	-1	-4	-1	0
P	-2	-1	-4	-4	-5	-1	-3	-4	2	-5	-5	-3	-4	-5	8	-2	-2	-5	0	-4
P	-2	-2	-2	-2	-4	0	-1	-4	-2	0	1	-1	2	0	5	-2	-2	-5	-3	0
E	-2	2	-2	2	-4	0	2	-4	-2	2	-2	-3	-2	-2	-1	3	1	-3	1	0
V	-2	-5	-5	-6	-3	-4	-5	-5	-5	3	2	-5	2	4	-5	-4	-3	-3	0	4
K	-2	2	1	0	2	1	1	-4	3	1	-2	3	0	-2	-4	-1	1	-1	1	-1
F	1	-5	-5	-5	-4	-5	-5	-5	-4	1	0	-5	-1	7	-5	-4	-3	-2	2	2
N	-4	-3	7	5	-5	-2	-1	-3	-2	-5	-4	-1	-4	-5	-4	-2	-2	-6	-5	-5
K	-3	6	-1	-3	-5	0	-1	-4	5	-5	-4	2	-3	-5	-4	-2	-2	-5	-3	-5
P	-2	-4	-4	-4	-5	-3	-3	-4	-4	-5	-5	-3	-5	-6	8	-1	-1	-6	-5	-4
F	-4	-5	-5	-6	-5	-5	-5	-5	-3	-2	-2	-5	-2	9	-6	-4	-4	-1	2	-3
V	-3	-4	-5	-6	-3	-3	-5	-6	-1	3	5	-4	2	1	-5	-4	-3	-4	-3	1
F	-3	-5	-5	-6	-1	-4	-5	-5	-4	2	2	-5	3	6	-5	-4	-3	-2	1	2
L	-1	-4	-5	-5	-3	-4	-5	-5	-4	3	3	-4	5	4	-5	-2	-1	-3	-1	1
M	-2	-5	-5	-5	-3	-5	-5	-6	-5	7	1	-5	2	-2	-5	-4	-3	-5	-3	2
I	-3	3	-3	-4	-1	-2	-1	-5	-2	0	0	0	0	3	-4	0	-1	1	4	1
E	-3	-3	0	5	-2	-1	4	-4	5	-5	-4	-2	-4	-5	-2	0	-3	-5	-3	-5
Q	-3	1	2	2	-5	0	3	-2	3	-2	-4	3	-1	-4	-2	-1	1	-1	-2	-1
N	-1	1	3	1	-4	0	1	-2	2	0	-3	1	-1	0	0	0	1	-4	0	-2
T	-1	-3	-1	-3	-3	-3	-3	-2	-1	0	-1	-2	-2	-4	-3	2	6	-5	-4	-1
K	-2	1	2	0	-5	3	0	3	1	-5	-5	2	-4	-3	-1	-1	-3	5	-3	-5
S	0	-2	0	-2	2	-3	-3	-2	0	0	-2	-3	0	-1	-3	5	2	-4	-2	0
P	-1	-4	-4	-2	-3	-3	-4	-5	-5	5	1	-4	-1	-3	4	0	-2	0	-4	2
L	-4	-4	-6	-6	-3	-4	-5	-6	-5	1	6	-5	0	0	-2	-5	-3	-4	-3	0
F	-4	-5	-5	-6	-4	-5	-5	-5	-3	-2	-1	-5	2	9	-6	-4	-4	-1	1	-3
M	-1	-4	-5	-5	1	-3	-4	-5	-4	1	3	-4	7	-2	-5	-4	-3	-4	-2	3
G	1	-4	-2	-3	-4	-4	-4	7	-4	-5	-4	-3	-4	-5	-4	0	-3	-5	-5	-5
K	-2	4	-2	-3	-5	2	-1	-4	1	-3	-4	6	-1	-5	-3	-1	-3	-5	-4	-4
V	-2	-5	-5	-5	-3	-4	-5	-5	-5	3	0	-4	1	0	-4	-4	-2	-4	-3	6

Fig. 2.3. Raw profile from PSI-Blast log file

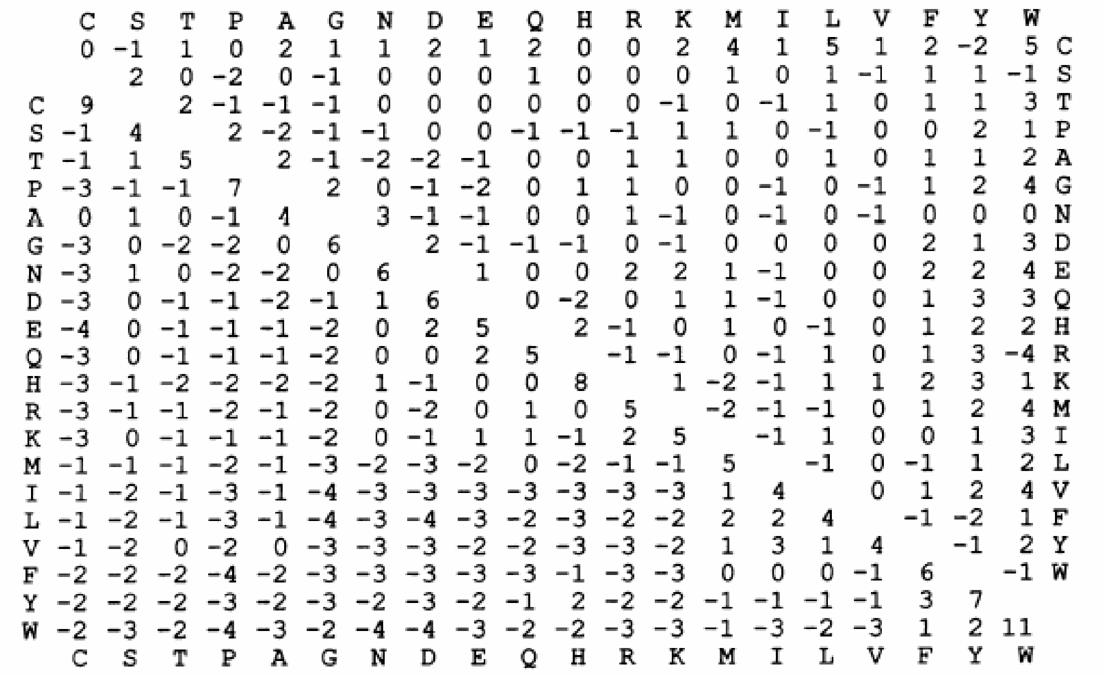

	C	S	T	P	A	G	N	D	E	Q	H	R	K	M	I	L	V	F	Y	W	
	0	-1	1	0	2	1	1	2	1	2	0	0	2	4	1	5	1	2	-2	5	C
		2	0	-2	0	-1	0	0	0	1	0	0	0	1	0	1	-1	1	1	-1	S
C	9		2	-1	-1	-1	0	0	0	0	0	0	-1	0	-1	1	0	1	1	3	T
S	-1	4		2	-2	-1	-1	0	0	-1	-1	-1	1	1	0	-1	0	0	2	1	P
T	-1	1	5		2	-1	-2	-2	-1	0	0	1	1	0	0	1	0	1	1	2	A
P	-3	-1	-1	7		2	0	-1	-2	0	1	1	0	0	-1	0	-1	1	2	4	G
A	0	1	0	-1	4		3	-1	-1	0	0	1	-1	0	-1	0	-1	0	0	0	N
G	-3	0	-2	-2	0	6		2	-1	-1	-1	0	-1	0	0	0	0	2	1	3	D
N	-3	1	0	-2	-2	0	6		1	0	0	2	2	1	-1	0	0	2	2	4	E
D	-3	0	-1	-1	-2	-1	1	6		0	-2	0	1	1	-1	0	0	1	3	3	Q
E	-4	0	-1	-1	-1	-2	0	2	5		2	-1	0	1	0	-1	0	1	2	2	H
Q	-3	0	-1	-1	-1	-2	0	0	2	5		-1	-1	0	-1	1	0	1	3	-4	R
H	-3	-1	-2	-2	-2	-2	1	-1	0	0	8		1	-2	-1	1	1	2	3	1	K
R	-3	-1	-1	-2	-1	-2	0	-2	0	1	0	5		-2	-1	-1	0	1	2	4	M
K	-3	0	-1	-1	-1	-2	0	-1	1	1	-1	2	5		-1	1	0	0	1	3	I
M	-1	-1	-1	-2	-1	-3	-2	-3	-2	0	-2	-1	-1	5		-1	0	-1	1	2	L
I	-1	-2	-1	-3	-1	-4	-3	-3	-3	-3	-3	-3	-3	1	4		0	1	2	4	V
L	-1	-2	-1	-3	-1	-4	-3	-4	-3	-2	-3	-2	-2	2	2	4		-1	-2	1	F
V	-1	-2	0	-2	0	-3	-3	-3	-2	-2	-3	-3	-2	1	3	1	4		-1	2	Y
F	-2	-2	-2	-4	-2	-3	-3	-3	-3	-3	-1	-3	-3	0	0	0	-1	6		-1	W
Y	-2	-2	-2	-3	-2	-3	-2	-3	-2	-1	2	-2	-2	-1	-1	-1	-1	3	7		
W	-2	-3	-2	-4	-3	-2	-4	-4	-3	-2	-2	-3	-3	-1	-3	-2	-3	1	2	11	
	C	S	T	P	A	G	N	D	E	Q	H	R	K	M	I	L	V	F	Y	W	

Fig. 2.4. BLOSUM 62 substitution matrix (Lower) and difference matrix (Upper) obtained by subtracting the PAM 160 matrix position by position. These matrices have identical relative entropies (0.70); the expected value of BLOSUM 62 is -0.52; that for PAM 160 is -0.57.

2.4 Quick Radial Basis Function Network

The radial basis function network (RBFN) is a special type of neural networks with several distinctive features [31]. Since its first proposal, the RBFN has attracted a high degree of interest in research communities. A RBFN consists of three layers, namely the input layer, the hidden layer, and the output layer. The input layer broadcasts the coordinates of the input vector to each of the nodes in the hidden layer. Each node in the hidden layer then produces an activation based on the associated radial basis function. Finally, each node in the output layer computes a linear combination of the activations of the hidden nodes. How a RBFN reacts to a given input stimulus is completely determined by the activation functions associated with the hidden nodes and the weights associated with the links between the hidden layer and the output layer. The general mathematical form of the output nodes in a RBFN is as follows:

$$c_j(x) = \sum_{i=1}^{k} w_{ji}\, \Phi(\, \|x - \mu_i\|; \sigma_i\,)\ ,$$

where $c_j(x)$ is the function corresponding to the j-th output unit (class-j) and is a linear combination of k radial basis functions $\Phi(\cdot)$ with center μ_i and bandwidth σ_i. Also, w_j is the weight vector of class-j and w_{ji} is the weight corresponding to the j-th class and i-th center. The general architecture of RBFN is shown in Fig. 2.5. It can be seen that constructing a RBFN involves determining the number of centers, k, the center locations, μ_i, the bandwidth of each center, σ_i, and the weights, w_{ji}. That is, training a RBFN involves determining the values of three sets of parameters: the centers (μ_i), the bandwidths (σ_i), and the weights (w_{ji}), in order to minimize a suitable cost function.

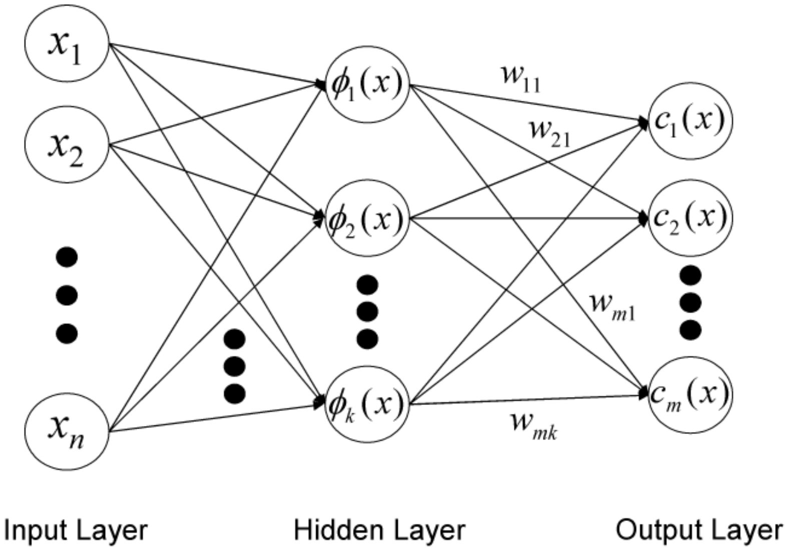

Fig. 2.5. General architecture of Radial Basis Function Network

In QuickRBF package [10], it is focused on the calculation of the weights, and conducting a simple method to determine the centers and bandwidths. Therefore, it selects the centers randomly in the package. Also, it utilizes a fixed bandwidth of each kernel function, which is set to five for each kernel function. After the centers and bandwidths of the kernel functions in the hidden layer have been determined, the transformation between the inputs and the corresponding outputs of the hidden units is now fixed. The network can thus be viewed as an equivalent single-layer network with linear output units. Then, the Least Mean Square Error method is used to determine the weights associated with the links between the hidden layer and the output layer.

Ou used a single-layer Quick Radial Basis Function Network [10] to analyze protein secondary structure with excellent prediction results on the RS126 data set. There are more details about QuickRBF can be found in QuickRBF package (http://csie.org/~yien/quickrbf/index.php). Here, we propose a modified QuickRBF system to predict protein relative solvent accessibility.

2.5 Coding Scheme

As with Hua and Sun’s work [32], the present analysis used the classical local coding scheme of the protein sequences with a sliding window. PSI-BLAST matrix with n rows and 20 columns can be defined for single sequence with n residues. For the first layer in the prediction, each residue is represented using 20 components in a vector, based on the PSSM. In order to allow a window to extend over the N-terminus and the C-terminus, an additional 21st unit (spacer) was attached to each residue. Then, each input vector has $21\times w$ components, where w is a sliding window size. For the second layer, the vector corresponding to a residue has four elements in the three-state prediction and three elements in the two-state prediction, where the first three elements represent the three relative solvent accessibility states, E, I, and B, in the three-state prediction and the first two elements represent the two relative solvent accessibility states, E and B, in the two-state prediction. Both the last units were added in order to allow a window to extend over the N-terminus and the C-terminus. If the window length is v, the dimension of the feature vector is $4\times v$ for the second layer in the three-state prediction and $3\times v$ in the two-state prediction.

2.6 Several Prediction System Structures

Five different kind of QuickRBF approaches are applied on three-state, E, I, and B, and two-state, E and B, relative solvent accessibility predictions. These five approaches include: (1) QuickRBF, (2) Two-Stage QuickRBF, (3) Common Fusion QuickRBF, (4) Local Tendency Fusion QuickRBF, and (5) Global Tendency Fusion QuickRBF.

2.6.1 QuickRBF Approach

A QuickRBF structure was used in the prediction system as shown in Fig. 2.6. The QuickRBF classifier classifies each residue of each sequence into the three relative solvent accessibility states, E, I, or B, by using the values of matrices of PSI-BLAST profile as the inputs. The outputs represent the tendency that the residue belongs to that state. The one-against-rest strategy was used for the multiclass classification, so each residue was classified into the state with the largest output value for a QuickRBF approach.

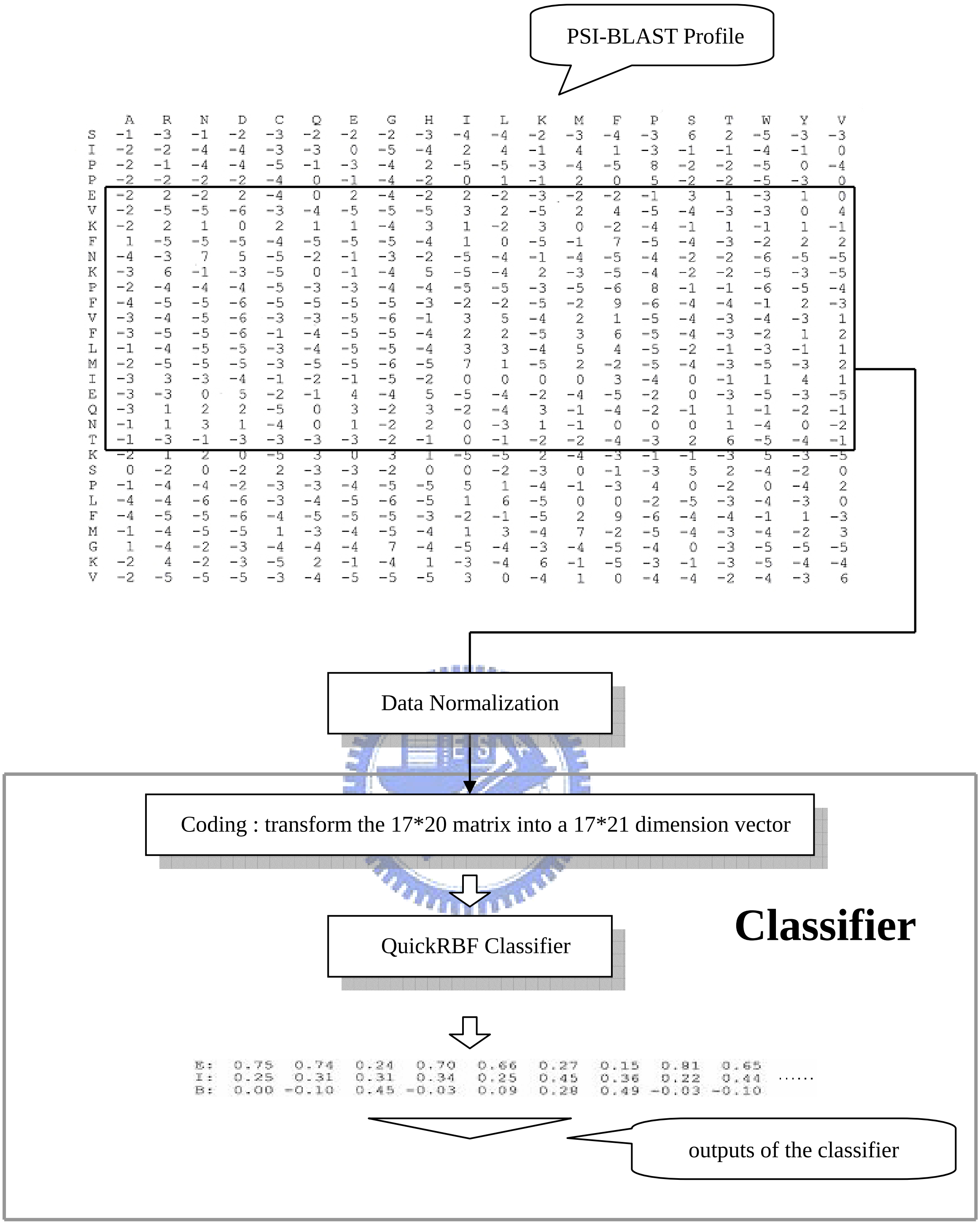

```
     A   R   N   D   C   Q   E   G   H   I   L   K   M   F   P   S   T   W   Y   V
S   -1  -3  -1  -2  -3  -2  -2  -2  -3  -4  -4  -2  -3  -4  -3   6   2  -5  -3  -3
I   -2  -2  -4  -4  -3  -3   0  -5  -4   2   4  -1   4   1  -3  -1  -1  -4  -1   0
P   -2  -1  -4  -4  -5  -1  -3  -4   2  -5  -5  -3  -4  -5   8  -2  -2  -5   0  -4
P   -2  -2  -2  -2  -4   0  -1  -4  -2   0   1  -1   2   0   5  -2  -2  -5  -3   0
E   -2   2  -2   2  -4   0   2  -4  -2   2  -2  -3  -2  -2  -1   3   1  -3   1   0
V   -2  -5  -5  -6  -3  -4  -5  -5  -5   3   2  -5   2   4  -5  -4  -3  -3   0   4
K   -2   2   1   0   2   1   1  -4   3   1  -2   3   0  -2  -4  -1   1  -1   1  -1
F    1  -5  -5  -5  -4  -5  -5  -5  -4   1   0  -5  -1   7  -5  -4  -3  -2   2   2
N   -4  -3   7   5  -5  -2  -1  -3  -2  -5  -4  -1  -4  -5  -4  -2  -2  -6  -5  -5
K   -3   6  -1  -3  -5   0  -1  -4   5  -5  -4   2  -3  -5  -4  -2  -2  -5  -3  -5
P   -2  -4  -4  -4  -5  -3  -3  -4  -4  -5  -5  -3  -5  -6   8  -1  -1  -6  -5  -4
F   -4  -5  -5  -6  -5  -5  -5  -5  -3  -2  -2  -5  -2   9  -6  -4  -4  -1   2  -3
V   -3  -4  -5  -6  -3  -3  -5  -6  -1   3   5  -4   2   1  -5  -4  -3  -4  -3   1
F   -3  -5  -5  -6  -1  -4  -5  -5  -4   2   2  -5   3   6  -5  -4  -3  -2   1   2
L   -1  -4  -5  -5  -3  -4  -5  -5  -4   3   3  -4   5   4  -5  -2  -1  -3  -1   1
M   -2  -5  -5  -5  -3  -5  -5  -6  -5   7   1  -5   2  -2  -5  -4  -3  -5  -3   2
I   -3   3  -3  -4  -1  -2  -1  -5  -2   0   0   0   0   3  -4   0  -1   1   4   1
E   -3  -3   0   5  -2  -1   4  -4   5  -5  -4  -2  -4  -5  -2   0  -3  -5  -3  -5
Q   -3   1   2   2  -5   0   3  -2   3  -2  -4   3  -1  -4  -2  -1   1  -1  -2  -1
N   -1   1   3   1  -4   0   1  -2   2   0  -3   1  -1   0   0   0   1  -4   0  -2
T   -1  -3  -1  -3  -3  -3  -3  -2  -1   0  -1  -2  -2  -4  -3   2   6  -5  -4  -1
K   -2   1   2   0  -5   3   0   3   1  -5  -5   2  -4  -3  -1  -1  -3   5  -3  -5
S    0  -2   0  -2   2  -3  -3  -2   0   0  -2  -3   0  -1  -3   5   2  -4  -2   0
P   -1  -4  -4  -2  -3  -3  -4  -5  -5   5   1  -4  -1  -3   4   0  -2   0  -4   2
L   -4  -4  -6  -6  -3  -4  -5  -6  -5   1   6  -5   0   0  -2  -5  -3  -4  -3   0
F   -4  -5  -5  -6  -4  -5  -5  -5  -3  -2  -1  -5   2   9  -6  -4  -4  -1   1  -3
M   -1  -4  -5  -5   1  -3  -4  -5  -4   1   3  -4   7  -2  -5  -4  -3  -4  -2   3
G    1  -4  -2  -3  -4  -4  -4   7  -4  -5  -4  -3  -4  -5  -4   0  -3  -5  -5  -5
K   -2   4  -2  -3  -5   2  -1  -4   1  -3  -4   6  -1  -5  -3  -1  -3  -5  -4  -4
V   -2  -5  -5  -5  -3  -4  -5  -5  -5   3   0  -4   1   0  -4  -4  -2  -4  -3   6
```

Data Normalization
Coding : transform the 17*20 matrix into a 17*21 dimension vector
QuickRBF Classifier
Classifier

```
E:  0.75  0.74  0.24  0.70  0.66  0.27  0.15  0.81  0.65
I:  0.25  0.31  0.31  0.34  0.25  0.45  0.36  0.22  0.44  ……
B:  0.00 -0.10  0.45 -0.03  0.09  0.28  0.49 -0.03 -0.10
```

Fig. 2.6. Architecture of QuickRBF method. The system includes two parts: the PSI-BLAST profile, and the classifier. The profile is transformed into a number of 21*17 dimension vectors using the slide-window method. These vectors are input into the QuickRBF classifier. The outputs of the QuickRBF classifier are a number of 3D vectors representing the tendency that the residue belongs to that state. The one-against-rest strategy was used to classify each residue into the state with the largest value.

2.6.2 Two-Stage QuickRBF Approach

A Two-Stage QuickRBF structure was used in the prediction system as shown in Fig. 2.7. The first stage is a QuickRBF classifier that classifies each residue of each sequence into the three relative solvent accessibility states, E, I, or B, by using the values of matrices of PSI-BLAST profile as the inputs. The outputs of the first stage represent the tendency that the residue belongs to that state. The second stage QuickRBF classifier also classifies each residue of each sequence into the three relative solvent accessibility states, E, I, or B, by using the RSA three-state tendency matrices from the outputs of the first stage as the inputs. The outputs of the second stage also represent the tendency that the residue belongs to that state. As with an One-Stage QuickRBF approach, the second stage also uses the one-against-rest strategy, with each residue classified into the state with the largest output value for a Two-Stage QuickRBF approach.

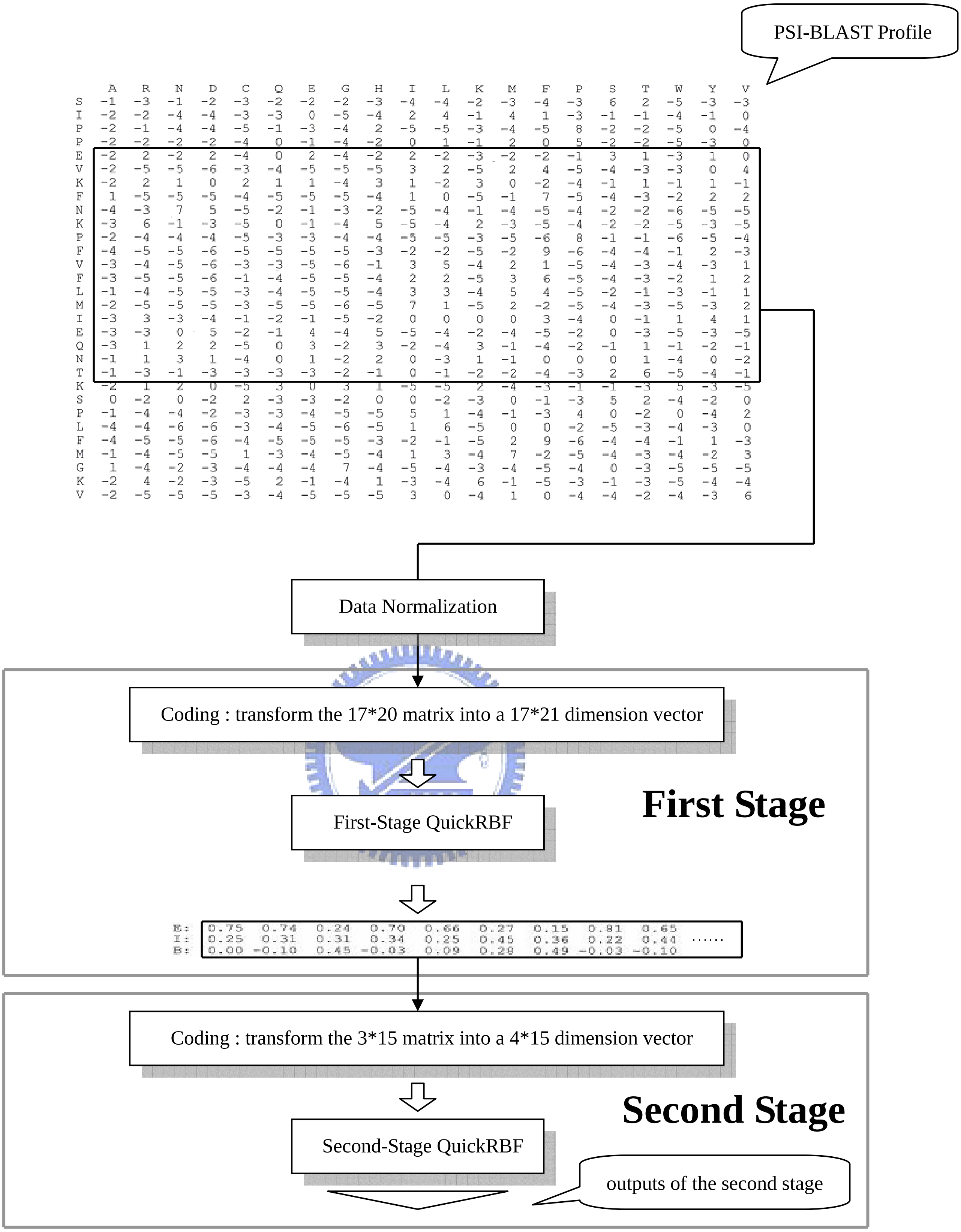
PSI-BLAST Profile
Data Normalization
Coding : transform the 17*20 matrix into a 17*21 dimension vector
First-Stage QuickRBF
First Stage
Coding : transform the 3*15 matrix into a 4*15 dimension vector
Second-Stage QuickRBF
Second Stage
outputs of the second stage

	A	R	N	D	C	Q	E	G	H	I	L	K	M	F	P	S	T	W	Y	V
S	-1	-3	-1	-2	-3	-2	-2	-2	-3	-4	-4	-2	-3	-4	-3	6	2	-5	-3	-3
I	-2	-2	-4	-4	-3	-3	0	-5	-4	2	4	-1	4	1	-3	-1	-1	-4	-1	0
P	-2	-1	-4	-4	-5	-1	-3	-4	2	-5	-5	-3	-4	-5	8	-2	-2	-5	0	-4
P	-2	-2	-2	-2	-4	0	-1	-4	-2	0	1	-1	2	0	5	-2	-2	-5	-3	0
E	-2	2	-2	2	-4	0	2	-4	-2	2	-2	-3	-2	-2	-1	3	1	-3	1	0
V	-2	-5	-5	-6	-3	-4	-5	-5	-5	3	2	-5	2	4	-5	-4	-3	-3	0	4
K	-2	2	1	0	2	1	1	-4	3	1	-2	3	0	-2	-4	-1	1	-1	1	-1
F	1	-5	-5	-5	-4	-5	-5	-5	-4	1	0	-5	-1	7	-5	-4	-3	-2	2	2
N	-4	-3	7	5	-5	-2	-1	-3	-2	-5	-4	-1	-4	-5	-4	-2	-2	-6	-5	-5
K	-3	6	-1	-3	-5	0	-1	-4	5	-5	-4	2	-3	-5	-4	-2	-2	-5	-3	-5
P	-2	-4	-4	-4	-5	-3	-3	-4	-4	-5	-5	-3	-5	-6	8	-1	-1	-6	-5	-4
F	-4	-5	-5	-6	-5	-5	-5	-5	-3	-2	-2	-5	-2	9	-6	-4	-4	-1	2	-3
V	-3	-4	-5	-6	-3	-3	-5	-6	-1	3	5	-4	2	1	-5	-4	-3	-4	-3	1
F	-3	-5	-5	-6	-1	-4	-5	-5	-4	2	2	-5	3	6	-5	-4	-3	-2	1	2
L	-1	-4	-5	-5	-3	-4	-5	-5	-4	3	3	-4	5	4	-5	-2	-1	-3	-1	1
M	-2	-5	-5	-5	-3	-5	-5	-6	-5	7	1	-5	2	-2	-5	-4	-3	-5	-3	2
I	-3	3	-3	-4	-1	-2	-1	-5	-2	0	0	0	0	3	-4	0	-1	1	4	1
E	-3	-3	0	5	-2	-1	4	-4	5	-5	-4	-2	-4	-5	-2	0	-3	-5	-3	-5
Q	-3	1	2	2	-5	0	3	-2	3	-2	-4	3	-1	-4	-2	-1	1	-1	-2	-1
N	-1	1	3	1	-4	0	1	-2	2	0	-3	1	-1	0	0	0	1	-4	0	-2
T	-1	-3	-1	-3	-3	-3	-3	-2	-1	0	-1	-2	-2	-4	-3	2	6	-5	-4	-1
K	-2	1	2	0	-5	3	0	3	1	-5	-5	2	-4	-3	-1	-1	-3	5	-3	-5
S	0	-2	0	-2	2	-3	-3	-2	0	0	-2	-3	0	-1	-3	5	2	-4	-2	0
P	-1	-4	-4	-2	-3	-3	-4	-5	-5	5	1	-4	-1	-3	4	0	-2	0	-4	2
L	-4	-4	-6	-6	-3	-4	-5	-6	-5	1	6	-5	0	0	-2	-5	-3	-4	-3	0
F	-4	-5	-5	-6	-4	-5	-5	-5	-3	-2	-1	-5	2	9	-6	-4	-4	-1	1	-3
M	-1	-4	-5	-5	1	-3	-4	-5	-4	1	3	-4	7	-2	-5	-4	-3	-4	-2	3
G	1	-4	-2	-3	-4	-4	-4	7	-4	-5	-4	-3	-4	-5	-4	0	-3	-5	-5	-5
K	-2	4	-2	-3	-5	2	-1	-4	1	-3	-4	6	-1	-5	-3	-1	-3	-5	-4	-4
V	-2	-5	-5	-5	-3	-4	-5	-5	-5	3	0	-4	1	0	-4	-4	-2	-4	-3	6

E:	0.75	0.74	0.24	0.70	0.66	0.27	0.15	0.81	0.65	
I:	0.25	0.31	0.31	0.34	0.25	0.45	0.36	0.22	0.44	……
B:	0.00	-0.10	0.45	-0.03	0.09	0.28	0.49	-0.03	-0.10	

Fig. 2.7. Architecture of Two-Stage QuickRBF method. The system includes three parts: the PSI-BLAST profile, the first stage, and the second stage. The profile is transformed into a number of 21*17 dimension vectors using the slide-window method. These vectors are input into the first-stage QuickRBF. The outputs of the first-stage QuickRBF are a number of 3D vectors representing the tendency that the residue belongs to that state. Using the slide-window method, the outputs of the first-stage QuickRBF are transformed into a number of 4*15 dimensional vector, which are used as the inputs of the second-stage QuickRBF. The final decisions are based on the outputs of the second-stage QuickRBF.

2.6.3 Common Fusion QuickRBF Approach

Three kind of fusion QuickRBF approaches were used to combine the outputs of a QuickRBF approach and the outputs of a Two-Stage QuickRBF approach. One is the Common Fusion QuickRBF approach, and the others are the Local Tendency Fusion QuickRBF approach and the Global Tendency Fusion QuickRBF approach. The architectures of these three approaches were illustrated in Figs. 2.8, 2.9, and 2.10. The common fusion strategy adds up the tendency outputs from a QuickRBF approach and the tendency outputs from a Two-Stage QuickRBF approach. Then we also use the one-against-rest strategy to classify each residue into the state with the largest value.

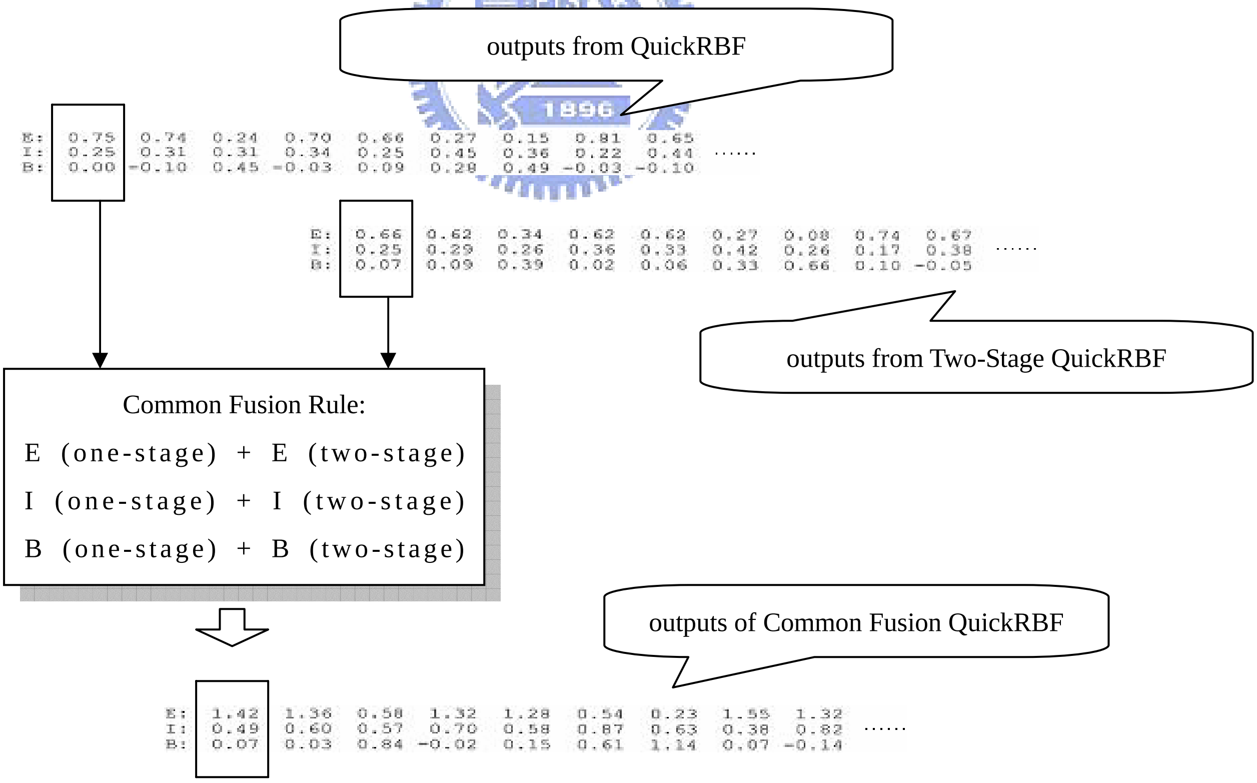
outputs from QuickRBF
E: 0.75 0.74 0.24 0.70 0.66 0.27 0.15 0.81 0.65
I: 0.25 0.31 0.31 0.34 0.25 0.45 0.36 0.22 0.44 ……
B: 0.00 -0.10 0.45 -0.03 0.09 0.28 0.49 -0.03 -0.10
E: 0.66 0.62 0.34 0.62 0.62 0.27 0.08 0.74 0.67
I: 0.25 0.29 0.26 0.36 0.33 0.42 0.26 0.17 0.38 ……
B: 0.07 0.09 0.39 0.02 0.06 0.33 0.66 0.10 -0.05
outputs from Two-Stage QuickRBF
Common Fusion Rule:
E (one-stage) + E (two-stage)
I (one-stage) + I (two-stage)
B (one-stage) + B (two-stage)
outputs of Common Fusion QuickRBF
E: 1.42 1.36 0.58 1.32 1.28 0.54 0.23 1.55 1.32
I: 0.49 0.60 0.57 0.70 0.58 0.87 0.63 0.38 0.82 ……
B: 0.07 0.03 0.84 -0.02 0.15 0.61 1.14 0.07 -0.14

Fig. 2.8. Architecture of Common Fusion QuickRBF method

2.6.4 Local Tendency Fusion QuickRBF Approach

The local tendency fusion strategy also adds up the tendency outputs from a QuickRBF approach and the tendency outputs from a Two-Stage QuickRBF approach. An occurrence number table is then applied in the summation as shown in Table 2.3. There are three occurrence numbers which are O_e, O_i and $O_{b,}$ where O_e means the numbers of exposed components in the test data, and O_i means the numbers of intermediate components in the test data, and O_b means the numbers of buried components in the test data. These three occurrence numbers represent the potential factors for the affection ability of the three relative solvent accessibility states. In other words, if an occurrence number is larger, the tendency of a residue which belongs to that state is larger. Then we also use the one-against-rest strategy to classify each residue into the state with the largest value.

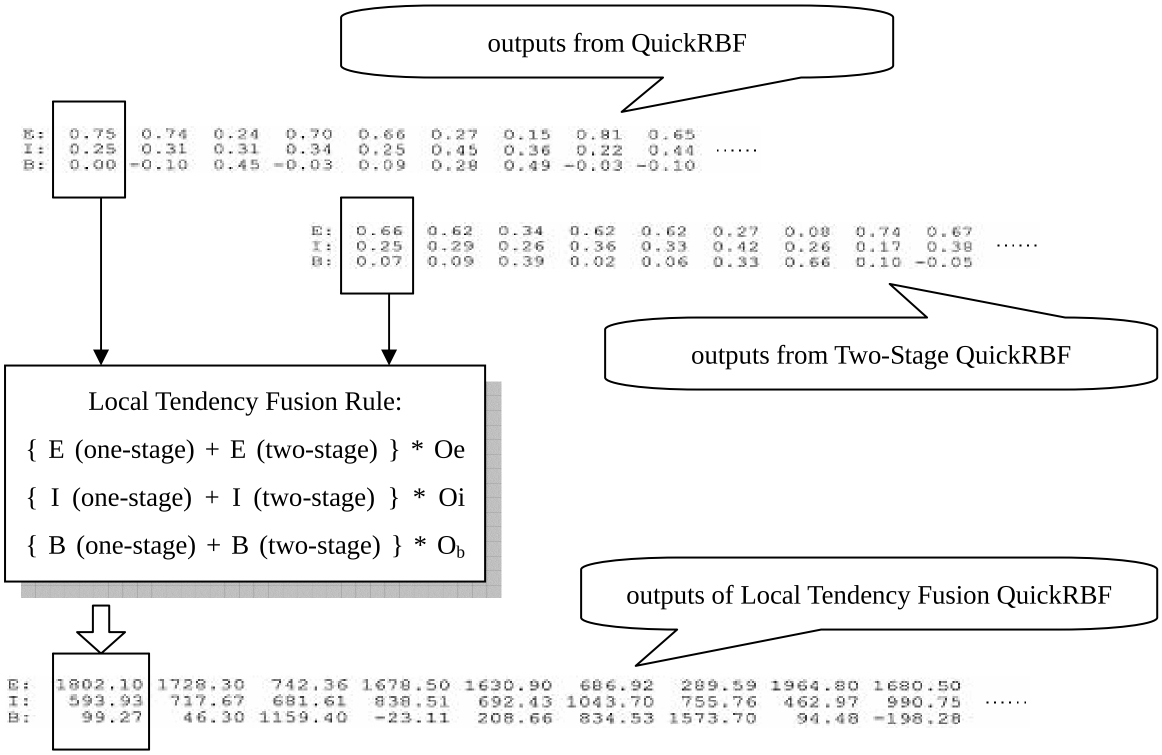

outputs from QuickRBF
outputs from Two-Stage QuickRBF
Local Tendency Fusion Rule:
{ E (one-stage) + E (two-stage) } * Oe
{ I (one-stage) + I (two-stage) } * Oi
{ B (one-stage) + B (two-stage) } * O_b
outputs of Local Tendency Fusion QuickRBF

```
E:  0.75  0.74  0.24  0.70  0.66  0.27  0.15  0.81  0.65
I:  0.25  0.31  0.31  0.34  0.25  0.45  0.36  0.22  0.44  ......
B:  0.00 -0.10  0.45 -0.03  0.09  0.28  0.49 -0.03 -0.10
```

```
E:  0.66  0.62  0.34  0.62  0.62  0.27  0.08  0.74  0.67
I:  0.25  0.29  0.26  0.36  0.33  0.42  0.26  0.17  0.38  ......
B:  0.07  0.09  0.39  0.02  0.06  0.33  0.66  0.10 -0.05
```

```
E:  1802.10 1728.30  742.36 1678.50 1630.90  686.92  289.59 1964.80 1680.50
I:   593.93  717.67  681.61  838.51  692.43 1043.70  755.76  462.97  990.75  ......
B:    99.27   46.30 1159.40  -23.11  208.66  834.53 1573.70   94.48 -198.28
```

Fig. 2.9. Architecture of Local Tendency Fusion QuickRBF method. These three occurrence numbers are based on each test fold.

Table 2.3. Occurrence numbers used for local and Global Tendency Fusion QuickRBF method. From Fold_A to Fold_G, these occurrence numbers of each fold are used for Local Tendency Fusion QuickRBF method. And the occurrence numbers of RS126 dataset are used for Global Tendency Fusion QuickRBF method.

Threshold: 9% ; 36%

component dataset	O_e	O_i	O_b	$O_e + O_i + O_b$
Fold_A	1524	1220	1532	4276
Fold_B	1441	1090	1174	3705
Fold_C	1269	1026	1169	3464
Fold_D	1436	1196	1222	3854
Fold_E	1081	829	961	2871
Fold_F	1036	835	900	2771
Fold_G	1271	1204	1376	3851
RS126	9058	7400	8334	24792

Threshold: 25%

component dataset	O_e	O_b	$O_e + O_b$
Fold_A	1983	2293	4276
Fold_B	1844	1861	3705
Fold_C	1629	1835	3464
Fold_D	1842	2012	3854
Fold_E	1400	1471	2871
Fold_F	1366	1405	2771
Fold_G	1709	2142	3851
RS126	11773	13019	24792

Table 2.3.(continued)

Threshold: 16%

component dataset	O_e	O_b	O_e + O_b
Fold_A	2373	1903	4276
Fold_B	2231	1474	3705
Fold_C	1977	1487	3464
Fold_D	2261	1593	3854
Fold_E	1679	1192	2871
Fold_F	1630	1141	2771
Fold_G	2083	1768	3851
RS126	14234	10558	24792

Threshold: 9%

component dataset	O_e	O_b	O_e + O_b
Fold_A	2744	1532	4276
Fold_B	2531	1174	3705
Fold_C	2295	1169	3464
Fold_D	2632	1222	3854
Fold_E	1910	961	2871
Fold_F	1871	900	2771
Fold_G	2475	1376	3851
RS126	16458	8334	24792

Table 2.3.(continued)

Threshold: 5%

component dataset	O_e	O_b	$O_e + O_b$
Fold_A	3028	1248	4276
Fold_B	2769	936	3705
Fold_C	2502	962	3464
Fold_D	2866	988	3854
Fold_E	2098	773	2871
Fold_F	2048	723	2771
Fold_G	2773	1078	3851
RS126	18084	6708	24792

Threshold: 0%

component dataset	O_e	O_b	$O_e + O_b$
Fold_A	3652	624	4276
Fold_B	3297	408	3705
Fold_C	3010	454	3464
Fold_D	3378	476	3854
Fold_E	2536	335	2871
Fold_F	2451	320	2771
Fold_G	3360	491	3851
RS126	21684	3108	24792

2.6.5 Global Tendency Fusion QuickRBF Approach

The global tendency fusion strategy is mostly the same with the local tendency fusion strategy. The difference between these two tendency fusion strategies is that these three occurrence numbers used for the global tendency fusion strategy are the occurrence numbers of three kind of components in the RS126 data set.

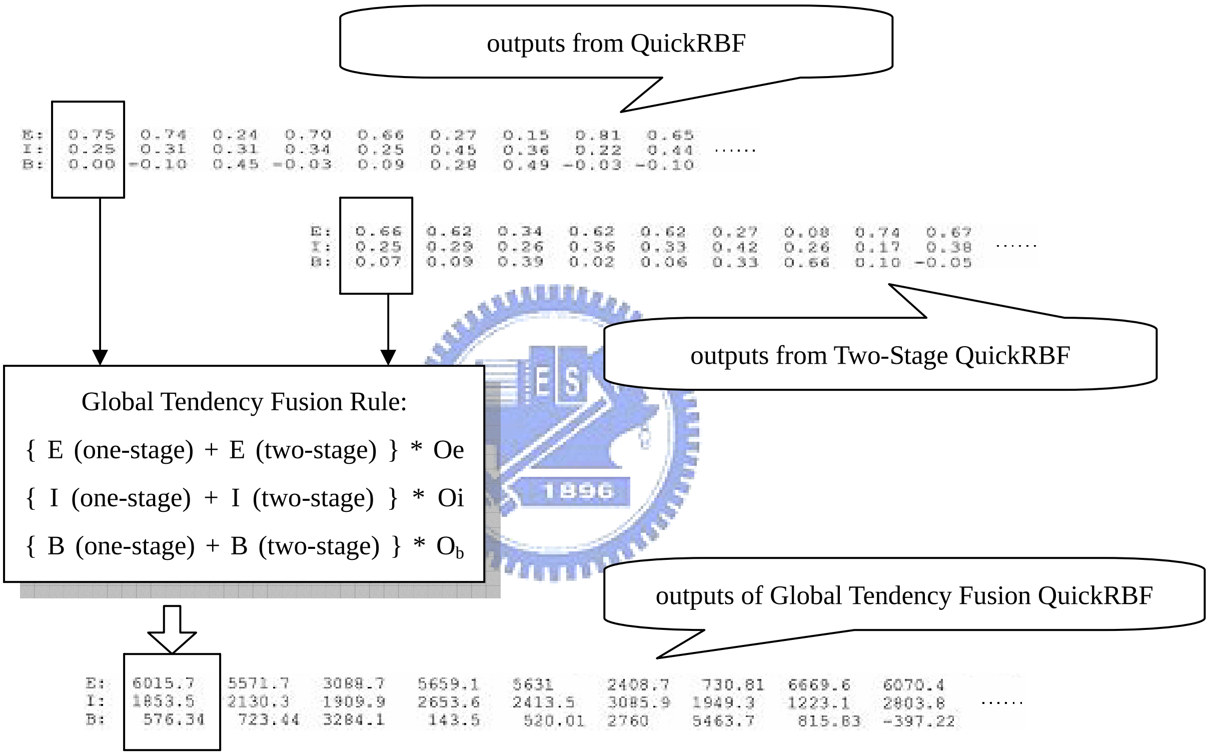
outputs from QuickRBF
outputs from Two-Stage QuickRBF
Global Tendency Fusion Rule:
{ E (one-stage) + E (two-stage) } * Oe
{ I (one-stage) + I (two-stage) } * Oi
{ B (one-stage) + B (two-stage) } * O_b
outputs of Global Tendency Fusion QuickRBF

```
E:  0.75  0.74  0.24  0.70  0.66  0.27  0.15  0.81  0.65
I:  0.25  0.31  0.31  0.34  0.25  0.45  0.36  0.22  0.44  ......
B:  0.00 -0.10  0.45 -0.03  0.09  0.28  0.49 -0.03 -0.10
```

```
E:  0.66  0.62  0.34  0.62  0.62  0.27  0.08  0.74  0.67
I:  0.25  0.29  0.26  0.36  0.33  0.42  0.26  0.17  0.38  ......
B:  0.07  0.09  0.39  0.02  0.06  0.33  0.66  0.10 -0.05
```

```
E:  6015.7   5571.7   3088.7   5659.1   5631     2408.7    730.81  6669.6   6070.4
I:  1853.5   2130.3   1909.9   2653.6   2413.5   3085.9   1949.3   1223.1   2803.8    ......
B:   576.34   723.44  3284.1    143.5    520.01  2760     5463.7    815.83  -397.22
```

Fig. 2.10. Architecture of Global Tendency Fusion QuickRBF method. These three occurrence numbers are based on the RS126 data set.

Chapter 3. Experiment and Simulation Results

3.1 Experiment Procedure of Five QuickRBF Approaches

Five different kind of QuickRBF approaches are applied on three-state, E, I, and B, and two-state, E and B, relative solvent accessibility predictions. These five methods are QuickRBF, Two-Stage QuickRBF, Common Fusion QuickRBF, Local Tendency Fusion QuickRBF, and Global Tendency Fusion QuickRBF.

For QuickRBF, One-Stage QuickRBF approach, each residue is coded as a 21-dimensional vector, where the first 20 elements of the vector are the corresponding elements in PSI-BLAST matrix and the last unit was added in order to allow a window to extend over the N- and the C-terminus. The window length is 17 and the dimension of the feature vector is 21×17. The number of the centers randomly selected from the training data set is 12000 and the bandwidth is five for each kernel function. The architecture of QuickRBF in the three-state prediction is shown previously in Fig. 2.6.

For Two-Stage QuickRBF, the window lengths are 17 for the first layer and 15 for the second layer. The dimension of the feature vector for the first layer is 21×17. The dimensions of the feature vectors for the second layer are 4×15 in the three-state prediction and 3×15 in the two-state prediction. The numbers of the centers randomly selected from the training data set are 12000 for the first layer and 500 for the second layer. The bandwidths are both five for the first and second layer. The architecture of Two-Stage QuickRBF in the three-state prediction is shown previously in Fig. 2.7.

These three kind of fusion strategies, Common Fusion, Local Tendency Fusion, and Global Tendency Fusion, are the combinations of One-Stage QuickRBF and Two-Stage QuickRBF. Different rules are used for each fusion strategy. The architectures of these three fusion strategies in the three-state prediction are shown previously in Figs. 2.8, 2.9, and 2.10.

3.2 Classification Accuracy of Five QuickRBF Approaches

The results and the comparison of the five different kind of QuickRBF approaches on RS126 data set are listed in Table 3.1. On the RS126 data set, QuickRBF gave the overall prediction accuracy 59.67% for the three-state prediction with respect to thresholds: 9%; 36% and 87.99%, 80.06%, 78.46%, 76.98%, 75.60%, respectively for the two-state prediction with respect to thresholds of 0%, 5%, 9%, 16%, 25%.

Two-Stage QuickRBF gave the overall prediction accuracy 59.11% for the three-state prediction with respect to thresholds: 9%; 36% and 87.55%, 79.25%, 78.21%, 76.15%, 73.76%, respectively for the two-state prediction with respect to thresholds of 0%, 5%, 9%, 16%, 25%.

Common Fusion QuickRBF gave the overall prediction accuracy 60.07% for the three-state prediction with respect to thresholds: 9%; 36% and 87.82%, 80.15%, 78.58%, 77.13%, 75.66%, respectively for the two-state prediction with respect to thresholds of 0%, 5%, 9%, 16%, 25%.

Local Tendency Fusion QuickRBF gave the overall prediction accuracy 59.91% for the three-state prediction with respect to thresholds: 9%; 36% and 87.60%, 77.20%, 75.84%, 76.54%, 75.55%, respectively for the two-state prediction with respect to thresholds of 0%, 5%, 9%, 16%, 25%.

Global Tendency Fusion QuickRBF gave the overall prediction accuracy 59.91% for the three-state prediction with respect to thresholds: 9%; 36% and 87.60%, 77.25%, 75.82%, 76.43%, 75.48%, respectively for the two-state prediction with respect to thresholds of 0%, 5%, 9%, 16%, 25%.

The accuracy plot of the above the five kind QuickRBF approaches is shown in Fig. 3.1 and Common Fusion QuickRBF is numbered three. Among these five QuickRBF approaches, Common Fusion QuickRBF has better performance for either the three-state prediction or the two-state prediction. Common Fusion QuickRBF is then decided as our modified QuickRBF approach because of the better performance among these five QuickRBF approaches.

Table 3.1. RSA classification accuracy of five kind QuickRBF methods on the RS126 data set with PSI-BLAST pssm profiles.

QuickRBF

accuracy: %

threshold dataset	3-state (9% ; 36%)	2-state (0%)	2-state (5%)	2-state (9%)	2-state (16%)	2-state (25%)
Fold_A	61.25	86.72	80.52	78.70	78.16	76.92
Fold_B	60.11	88.77	81.30	79.65	77.84	76.06
Fold_C	62.99	87.90	81.76	81.18	79.19	77.77
Fold_D	59.37	88.53	80.95	79.09	77.09	75.61
Fold_E	60.85	88.65	81.92	80.22	78.65	76.63
Fold_F	59.11	89.03	81.60	79.18	76.18	74.27
Fold_G	53.99	86.32	72.34	71.18	71.75	71.90
Average	**59.67**	**87.99**	**80.06**	**78.46**	**76.98**	**75.60**

Two-Stage QuickRBF

accuracy: %

threshold dataset	3-state (9% ; 36%)	2-state (0%)	2-state (5%)	2-state (9%)	2-state (16%)	2-state (25%)
Fold_A	60.71	86.62	80.43	78.30	76.52	74.58
Fold_B	60.59	88.18	78.11	78.79	76.73	75.17
Fold_C	62.73	88.14	81.41	81.21	77.34	77.74
Fold_D	57.16	88.30	79.94	78.15	75.71	72.00
Fold_E	59.80	88.92	81.85	80.49	77.81	72.34
Fold_F	58.72	88.92	80.04	77.55	75.78	72.21
Fold_G	54.06	83.80	72.97	72.97	73.18	72.29
Average	**59.11**	**87.55**	**79.25**	**78.21**	**76.15**	**73.76**

Table 3.1. (continued)

Common Fusion QuickRBF

						accuracy: %
threshold dataset	3-state (9% ; 36%)	2-state (0%)	2-state (5%)	2-state (9%)	2-state (16%)	2-state (25%)
Fold_A	61.20	86.67	80.40	78.53	77.95	76.19
Fold_B	61.27	88.88	80.59	79.54	78.19	76.90
Fold_C	63.40	88.08	81.67	81.67	78.96	78.09
Fold_D	59.06	88.43	80.83	78.54	76.93	74.73
Fold_E	61.20	88.75	82.41	80.74	78.34	76.04
Fold_F	59.33	88.70	81.81	78.85	76.69	74.92
Fold_G	55.05	85.23	73.36	72.16	72.84	72.76
Average	**60.07**	**87.82**	**80.15**	**78.58**	**77.13**	**75.66**

Local Tendency Fusion QuickRBF

						of accuracy: %
threshold dataset	3-state (9% ; 36%)	2-state (0%)	2-state (5%)	2-state (9%)	2-state (16%)	2-state (25%)
Fold_A	60.69	85.45	76.38	75.89	75.96	76.31
Fold_B	60.89	88.99	79.00	77.11	77.30	76.87
Fold_C	62.96	87.01	78.41	78.03	79.27	78.38
Fold_D	59.70	87.68	78.20	76.99	77.19	74.18
Fold_E	60.92	88.30	78.44	77.01	77.85	75.62
Fold_F	59.18	88.49	78.20	77.05	76.15	74.77
Fold_G	55.03	87.25	71.80	68.79	72.06	72.73
Average	**59.91**	**87.60**	**77.20**	**75.84**	**76.54**	**75.55**

Table 3.1. (continued)

Global Tendency Fusion QuickRBF

accuracy: %

threshold dataset	3-state (9% ; 36%)	2-state (0%)	2-state (5%)	2-state (9%)	2-state (16%)	2-state (25%)
Fold_A	60.29	85.48	76.08	75.07	75.16	76.61
Fold_B	61.16	89.02	79.16	77.38	77.92	76.65
Fold_C	63.05	87.01	78.32	78.06	79.30	78.32
Fold_D	59.68	87.68	78.41	77.43	77.30	74.16
Fold_E	60.89	88.26	78.44	77.05	78.23	75.44
Fold_F	59.26	88.49	78.49	77.27	76.18	74.67
Fold_G	55.05	87.25	71.88	68.50	70.89	72.50
Average	**59.91**	**87.60**	**77.25**	**75.82**	**76.43**	**75.48**

Comparison of five kind QuickRBF methods

accuracy: %

threshold method	3-state (9% ; 36%)	2-state (0%)	2-state (5%)	2-state (9%)	2-state (16%)	2-state (25%)
QuickRBF	59.67	87.99	80.06	78.46	76.98	75.60
Two-Stage QuickRBF	59.11	87.55	79.25	78.21	76.15	73.76
Common Fusion QuickRBF	60.07	87.82	80.15	78.58	77.13	75.66
Local Tendency Fusion QuickRBF	59.91	87.60	77.20	75.84	76.54	75.55
Global Tendency Fusion QuickRBF	59.91	87.60	77.25	75.82	76.43	75.48

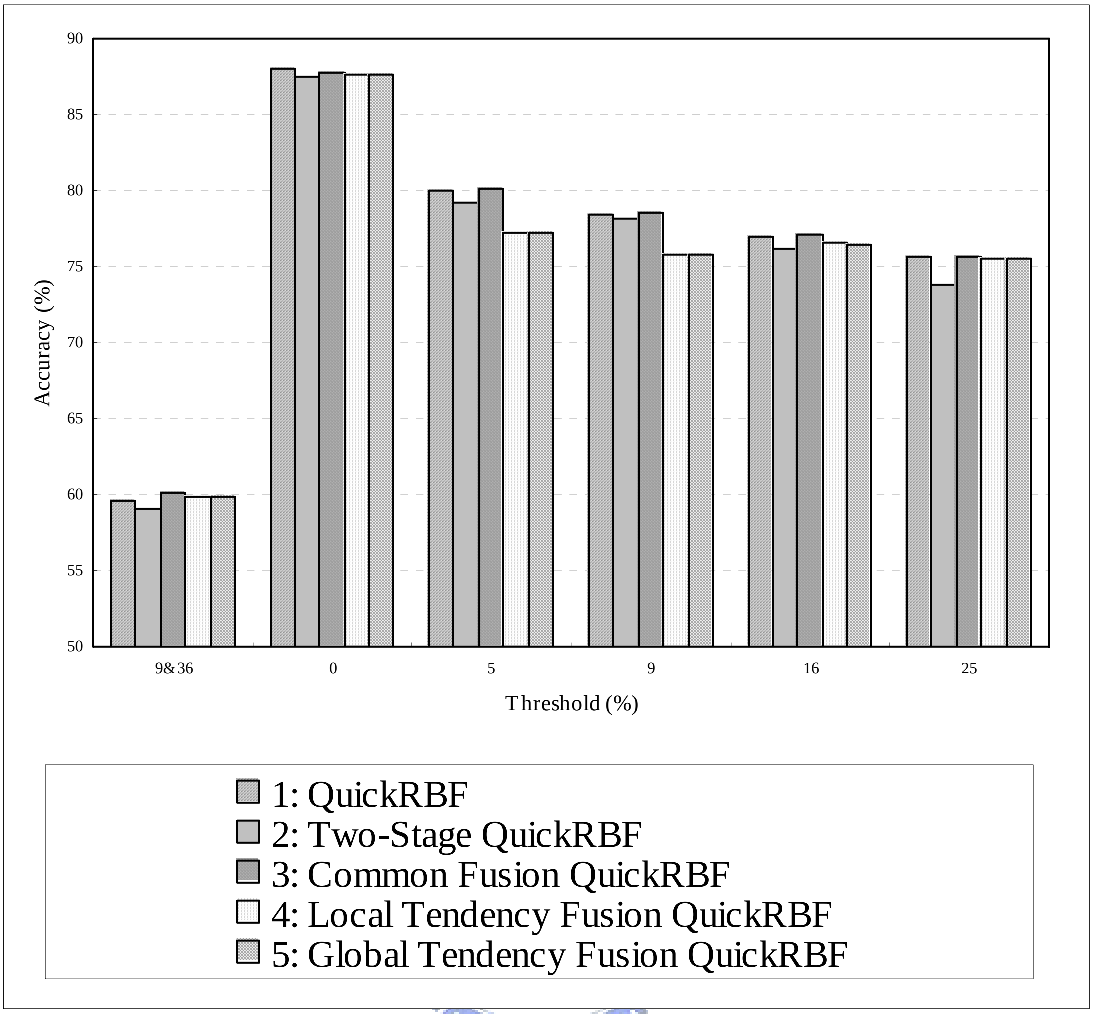

Fig. 3.1. Accuracy plot of five kind QuickRBF methods.

3.3 Matthew’s Correlation Coefficients of Five QuickRBF Approaches

Another measure used to evaluate the performance of prediction methods is the Matthew’s Correlation Coefficient (MCC). It can be calculated from an accuracy table *A* by the following equations:

A_{ij} = number of residues predicted to be in type *j* and observed to be in type *i*,

$$MCC_i = \frac{p_i n_i - u_i o_i}{\sqrt{(p_i + u_i)(p_i + o_i)(n_i + u_i)(n_i + o_i)}},$$

$$p_i = A_{ii},$$

$$n_i = \sum_{j \neq i}^{3} \sum_{k \neq i}^{3} A_{jk},$$

$$o_i = \sum_{j \neq i}^{3} A_{ji},$$

$$u_i = \sum_{j \neq i}^{3} A_{ij}, \text{ for } i = \text{E, I, B.}$$

Also, p_i , n_i , o_i and u_i are the number of true positives, true negatives, false positives and false negatives for class *i*, respectively. The MCCs have the same value for the two classes in the case of the two-state prediction, i.e. $\text{MCC}_\text{E} = \text{MCC}_\text{B}$.

First, the accuracy tables *A* of Common Fusion QuickRBF on each fold and the RS126 data set is shown in Table 3.2. Then, the MCCs of five kind QuickRBF methods on the RS126 data set is shown in Table 3.3. In a similar trend as Table 3.1, MCC’s of Common Fusion QuickRBF usually perform well, although not always the best, in comparison to other QuickRBF approaches.

Table 3.2. The accuracy tables *A* of Common Fusion QuickRBF on each fold and RS126.

3-state (9%; 36%)

	A_{EE}	A_{II}	A_{BB}	A_{EI}	A_{EB}	A_{IE}	A_{IB}	A_{BE}	A_{BI}
Fold_A	1276	294	1042	141	107	587	339	277	213
Fold_B	1134	285	837	187	120	455	350	144	193
Fold_C	1033	257	905	130	106	433	336	138	126
Fold_D	1067	276	940	180	189	433	487	145	137
Fold_E	843	196	724	132	106	347	286	120	117
Fold_F	816	170	645	113	107	387	278	155	100
Fold_G	835	279	1011	207	229	434	491	174	191
RS126	7004	1757	6104	1090	964	3076	2567	1153	1077

2-state (25%)

	A_{EE}	A_{BB}	A_{EB}	A_{BE}
Fold_A	1695	1563	288	730
Fold_B	1417	1432	427	429
Fold_C	1247	1458	382	377
Fold_D	1244	1636	598	376
Fold_E	952	1231	448	240
Fold_F	996	1080	370	325
Fold_G	1109	1693	600	449
RS126	8660	10093	3113	2926

2-state (16%)

	A_{EE}	A_{BB}	A_{EB}	A_{BE}
Fold_A	2134	1199	239	704
Fold_B	1842	1055	389	419
Fold_C	1613	1122	364	365
Fold_D	1803	1162	458	431
Fold_E	1402	847	277	345
Fold_F	1368	757	262	384
Fold_G	1596	1209	487	559
RS126	11758	7351	2476	3207

Table 3.2. (continued)

2-state (9%)

	A_{EE}	A_{BB}	A_{EB}	A_{BE}
Fold_A	2489	869	255	663
Fold_B	2228	719	303	455
Fold_C	2051	778	244	391
Fold_D	2300	727	332	495
Fold_E	1742	576	168	385
Fold_F	1657	528	214	372
Fold_G	2003	776	472	600
RS126	14470	4973	1988	3361

2-state (5%)

	A_{EE}	A_{BB}	A_{EB}	A_{BE}
Fold_A	2818	620	210	628
Fold_B	2449	537	320	399
Fold_C	2259	570	243	392
Fold_D	2660	455	206	533
Fold_E	1939	427	159	346
Fold_F	1885	382	163	341
Fold_G	2245	580	528	498
RS126	16255	3571	1829	3137

2-state (0%)

	A_{EE}	A_{BB}	A_{EB}	A_{BE}
Fold_A	3612	94	40	530
Fold_B	3206	87	91	321
Fold_C	2956	95	54	359
Fold_D	3330	78	48	398
Fold_E	2473	75	63	260
Fold_F	2416	42	35	278
Fold_G	3202	80	158	411
RS126	21195	551	489	2557

Table 3.3. Matthew's Correlation Coefficients of Five Kind QuickRBF Methods on RS126.

3-state (9%; 36%)			
MCC / method	MCC_E	MCC_I	MCC_B
QuickRBF	0.477	0.146	0.500
Two-Stage QuickRBF	0.485	0.130	0.491
Common Fusion QuickRBF	0.488	0.142	0.502
Local Tendency Fusion QuickRBF	0.487	0.123	0.508
Global Tendency Fusion QuickRBF	0.489	0.123	0.505

2-state (25%)	
MCC / method	$MCC_E = MCC_B$
QuickRBF	0.517
Two-Stage QuickRBF	0.476
Common Fusion QuickRBF	0.511
Local Tendency Fusion QuickRBF	0.439
Global Tendency Fusion QuickRBF	0.440

2-state (16%)	
MCC / method	$MCC_E = MCC_B$
QuickRBF	0.524
Two-Stage QuickRBF	0.512
Common Fusion QuickRBF	0.528
Local Tendency Fusion QuickRBF	0.514
Global Tendency Fusion QuickRBF	0.514

Table 3.3. (continued)

2-state (9%)	
MCC method	$MCC_E = MCC_B$
QuickRBF	0.493
Two-Stage QuickRBF	0.499
Common Fusion QuickRBF	0.500
Local Tendency Fusion QuickRBF	0.513
Global Tendency Fusion QuickRBF	0.513

2-state (5%)	
MCC method	$MCC_E = MCC_B$
QuickRBF	0.449
Two-Stage QuickRBF	0.457
Common Fusion QuickRBF	0.464
Local Tendency Fusion QuickRBF	0.482
Global Tendency Fusion QuickRBF	0.483

2-state (0%)	
MCC method	$MCC_E = MCC_B$
QuickRBF	0.249
Two-Stage QuickRBF	0.262
Common Fusion QuickRBF	0.256
Local Tendency Fusion QuickRBF	0.281
Global Tendency Fusion QuickRBF	0.281

3.4 Comparison with other Approaches

Comparison of performance of modified QuickRBF approach with other methods in RSA prediction on the RS126 data set is shown in Table 3.4. Accuracy plot of modified QuickRBF approach and other methods is shown in Fig. 3.2.

Modified QuickRBF, Common Fusion, is our method, and reported 60.1% for the three-state prediction with respect to 9%; 36% thresholds, and 87.8%, 80.2%, 78.6%, 77.1%, 75.7%, respectively for the two-state predictions with respect to thresholds of 0%, 5%, 9%, 16%, 25%.

Fuzzy *k*-NN (Sim**,** Kim and Lee**,** 2005) used fuzzy *k*-nearest neighbor method [23] using PSI-BLAST profiles as feature vectors, and shows slightly better prediction accuracies than other methods on the RS126 data set ,and reported 63.8% for the three-state prediction with respect to 9%; 36% thresholds, and 87.2%, 82.2%, 79.0%, 78.3%, respectively for the two-state predictions with respect to thresholds of 0%, 5%, 16%, 25%.

PHDacc (Rost and Sander, 1994) used a neural network method [3] using evolutionary profiles of amino acid substitutions derived from multiple sequence alignments, and reported 57.5% for the three-state prediction with respect to 9%; 36% thresholds, and 86.0%, 74.6%, 75.0%, respectively for the two-state predictions with respect to thresholds of 0%, 9%, 16%.

SVMpsi (Kim and Park, 2004) was based on a support vector machine [21] using the position-specific scoring matrix generated from PSI-BLAST, and reported 59.6% accuracy for the three-state prediction with respect to 9%; 36% thresholds and 86.2%, 79.8%, 77.8%, 76.8%, respectively accuracies for the two-state predictions with respect to thresholds of 0%, 5%, 16%, 25%.

Two-Stage SVMpsi (Nguyen and Rajapakse, 2005) used a Two-Stage SVMpsi approach [22] using the position-specific scoring matrix generated from PSI-BLAST, and reported 90.2%, 83.5%, 81.3%, 79.4%, respectively accuracies for the two-state predictions with respect to thresholds of 0%, 5%, 9%, 16%. These prediction accuracies are obtained from their published results. The three state accuracy of Modified QuickRBF is 60.1%, which is 3.7% lower than Fuzzy *k*-NN (63.8%) and 0.5% higher than SVMpsi (59.6%).

Table 3.4. Comparison of performance of modified QuickRBF approach with other methods in RSA prediction on the RS126 data set with PSSMs generated by PSI-BLAST.

accuracy: %

threshold	3-state	2-state	2-state	2-state	2-state	2-state
method	(9%; 36%)	(0%)	(5%)	(9%)	(16%)	(25%)
Modified QuickRBF (Common Fusion)	60.1	87.8	80.2	78.6	77.1	75.7
PHDacc	57.5	86.0	—	74.6	75.0	—
SVMpsi	59.6	86.2	79.8	—	77.8	76.8
Two-Stage SVMpsi	—	90.2	83.5	81.3	79.4	—
Fuzzy *k*-NN	63.8	87.2	82.2	—	79.0	78.3

PHDacc (Rost and Sander, 1994) used neural networks [3].

SVMpsi (Kim and Park, 2004) was based on support vector machine [21].

Two-Stage SVMpsi (Nguyen and Rajapakse, 2005) used a two-stage SVM approach [22].

Fuzzy *k*-NN (Sim, Kim and Lee, 2005) used fuzzy k-nearest neighbor method [23].

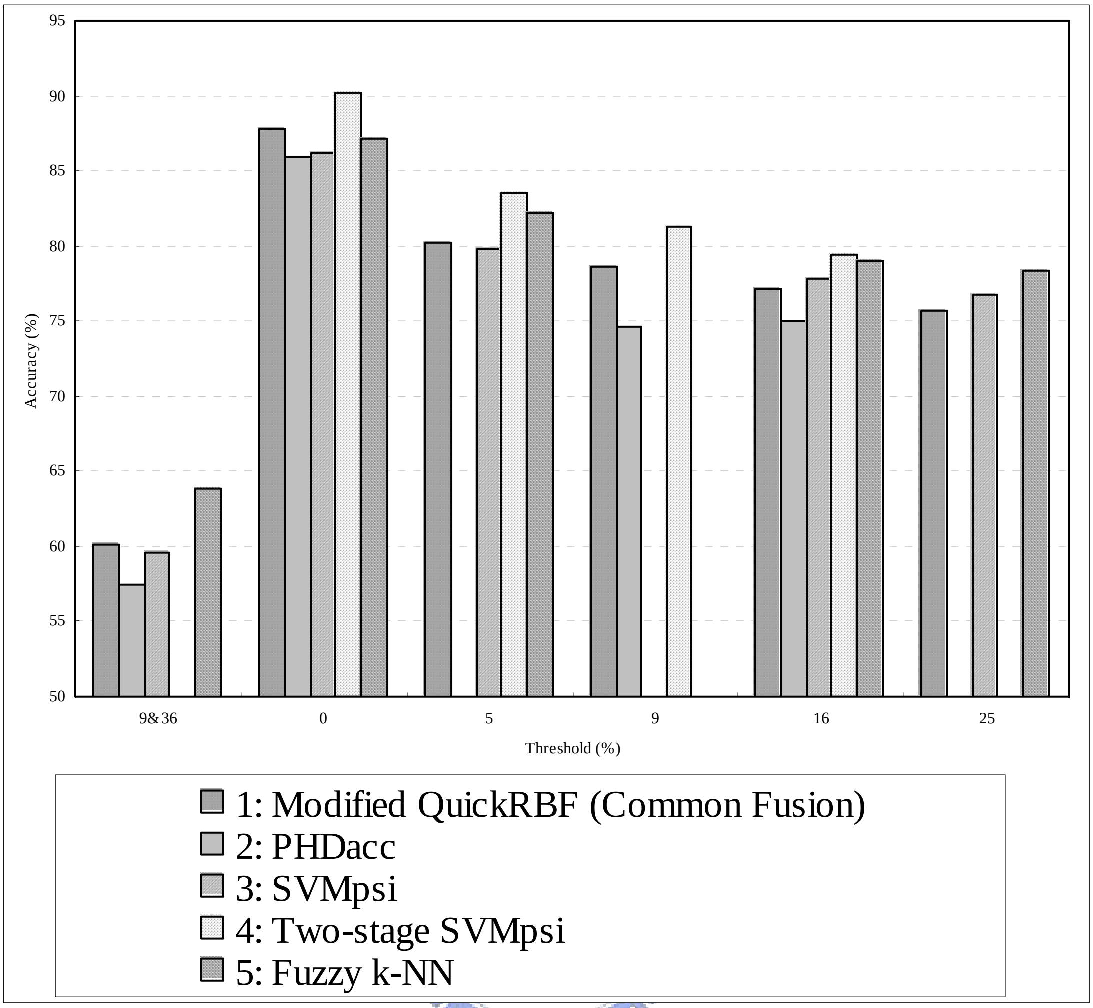

Fig. 3.2. Accuracy plot of Modified QuickRBF and other methods.

Chapter 4. Conclusion and Discussion

In this study, we have applied the five QuickRBF approaches, which are QuickRBF, Two-Stage QuickRBF, Common Fusion QuickRBF, Local Tendency Fusion QuickRBF, and Global Tendency Fusion QuickRBF, to predict relative solvent accessibility, using PSI-BLAST profiles as feature vectors. Our best method, Common Fusion QuickRBF, achieved the similar performance as the researches did in the recent years. Because the goal of this thesis was to provide a new approach for relative solvent accessibility, the results suggest that the modified QuickRBF approach is a successful one.

In the future strategy, we can apply our method on a larger data set. Data set growth can give an indirect advantage to our method. And our modified QuickRBF approach can be selected as a method to combine with other methods.

References

[1] J. Chandonia and M. Karplus, “New methods for accurate prediction of protein secondary structure,” *Protein Engineering*, vol. 35, pp. 293–306, 1999.

[2] D.W. Mount, “Bioinformatics: sequence and genome analysis,” *Cold Spring Harbor, NY: Cold Spring Harbor Laboratory Press*, 2001.

[3] B. Rost and C. Sander, “Conservation and prediction of solvent accessibility in protein families,” *Proteins*, vol. 20, pp. 216–226, 1994.

[4] M.J. Thompson and R.A. Goldstein, “Predicting solvent accessibility: higher accuracy using Bayesian statistics and optimized residue substitution classes,” *Proteins*, vol. 47, pp. 142–153, 1996.

[5] S. Pascarella, R.D. Persio, F. Bossa, and P. Argos, “Easy method to predict solvent accessibility from multiple protein sequence alignments,” *Proteins*, vol. 32, pp. 190–199, 1999.

[6] X. Li and X.M. Pan, “New method for accurate prediction of solvent accessibility from protein sequence,” *Proteins*, vol. 42, pp. 1–5, 2001.

[7] G. Pollastri, P. Baldi, P. Fariselli, and R. Casadio, “Prediction of coordination number and relative solvent accessibility in proteins,” *Proteins*, vol. 47, pp. 142–153, 2002.

[8] S. Ahmad and M.M. Gromiha, “NETASA: neural network based prediction of solvent accessibility,” *Bioinformatics*, vol. 18, pp. 819–824, 2002.

[9] H. Naderi-Manesh, M. Sadeghi, S. Araf, and A.A.M. Movahedi, “Predicting of protein surface accessibility with information theory,” *Proteins*, vol. 42, pp. 452–459, 2001.

[10] Y.Y. Ou, "QuickRBF is an Efficient Construction of Radial Basis Function Networks with the Cholesky Decomposition," *http://csie.org/~yien/quickrbf/* .

[11] J.D. Bernal, I. Fankuchen, and M. Perutz, "An X-Ray study of chymotrypsin and haemoglobin," *Nature*, vol. 141, pp. 523–524, 1938.

[12] W.A. Kauzmann, "Some factors in the interpretation of protein denaturation," *Protein Chem.*, vol. 14, pp. l–63, 1959.

[13] B.K. Lee and F.M. Richards, "The interpretation of protein structures: estimation of static accessibility," *J. Mol. Biol.*, vol. 55, pp. 379–400, 1971.

[14] C. Chothia, "The nature of the accessible and buried surfaces in proteins," *J. Mol. Biol.*, vol. 105, pp. 1–12, 1976.

[15] M.L. Connolly, "Solvent-accessible surfaces of proteins and nucleic acids," *Science*, vol. 221, pp. 709–713, 1983.

[16] W. Kabsch and C. Sander, "Dictionary of protein secondary structure: pattern recognition of hydrogen-bonded and geometrical features," *Biopolymers*, vol. 22, pp. 2577–2637, 1983.

[17] J. Janin, "Surface and inside volumes in globular proteins," *Nature*, vol. 277, pp. 491–492, 1979.

[18] G.D. Rose, A.R. Geselowitz, G.J. Lesser, R.H. Lee, and M.H. Zehfus, "Hydrophobicity of amino acid residues in globular proteins," *Science*, vol. 229, pp. 834–838, 1985.

[19] C. Sander, M. Scharf, and R. Schneider, "Design of protein structures in: Protein Engineering: A practical Approach," *Oxford University press*, pp. 89–115, 1992

[20] H. Hirakawa and S. Kuhara, "Prediction of Hydrophobic Cores of Proteins Using Wavelet Analysis," *Genome Inform Ser Workshop Genome Information*, vol. 8, pp. 61–70, 1997

[21] H. Kim and H. Park, “Prediction of protein relative solvent accessibility with support vector machines,” *Proteins*, vol. 54, pp. 557–562, 2004.

[22] M.N. Nguyen and J.C. Rajapakse, “Prediction of protein relative solvent accessibility with a two-stage SVM approach,” *Proteins*, vol. 59, pp. 30–37, 2005.

[23] J. Sim, S.Y. Kim, and J. Lee, “Prediction of protein solvent accessibility using fuzzy k-nearest neighbor method,” *Bioinformatics*, vol. 21, pp. 2844–2849, 2005.

[24] D.T. Jones, “Protein secondary structure prediction based on position specific scoring matrices,” *J. Mol. Biol.*, vol. 292, pp. 195–202, 1999.

[25] B. Rost and C. Sander, “Combining evolutionary information and neural networks to predict protein secondary structure,” *Proteins*, vol. 19, pp. 55–72, 1994.

[26] G.J. Barton, “Protein secondary structure prediction,” *Curr. Opin. Struct. Biol.*, vol. 5, pp. 372–376, 1995.

[27] P. Baldi, S. Brunak, P. Frasconi, G. Pollastri, and G. Soda, “Exploiting the past and the future in protein secondary structure prediction,” *Bioinformatics*, vol. 15, pp. 937–946, 1999.

[28] S.F. Altschul *et al.*, “Gapped BLAST and PSI-BLAST: a new generation of protein database search programs,” *Nucleic Acids Res.*, vol. 25, pp. 3389–3402, 1997.

[29] D.T. Jones, “Protein secondary structure prediction based on position-specific scoring matrices,” *J. Mol. Biol.*, vol. 292, pp. 195–202, 1999.

[30] S. Henikoff and J.G. Henikoff, “Amino acid substitution matrices from protein blocks,” *Proc. Natl. Acad. Sci.*, vol. 89, pp. 10915–10919, 1992.

[31] T**.** Poggio and F. Girosi, “A sparse representation for function approximation,” *Neural Comput.*, vol. 10, pp. 1445–1454, 1998.

[32] S. Hua and Z. Sun, “A novel method of protein secondary structure prediction with high segment overlap measure: support vector machine approach,” *J. Mol. Biol.*, vol. 308, pp. 397–407, 2001.